THE MEASUREMENT OF TIME DEPENDENT POISSON'S RATIO

Master's Report by

TONNY SOESANTO

In Partial Fulfillment of the
Requirements for the degree of

M A S T E R O F S C I E N C E

California Institute of Technology
Pasadena, California

1982

To my mother, family, and Fee Lan

ACKNOWLEDGMENT

I would like to express my sincerest gratitude to Dr. Tschoegl for his advice, support, encouragement, and patience during my work here at Caltech. I enjoy working with him very much and his guidance will certainly brighten my future career. Mrs. Tschoegl's kindness is also very much appreciated.

I would like to thank my office-mates, Bill Moonan and Cigdem Gurer for providing much needed help and advice. They have been such good friends in sharing my frustration and joy. I wish them good luck in their future careers. I also thank Herb Adam, John Powell, and others who contributed many ideas and efforts in this project.

My deepest thanks goes to Rita Mendelson who did such a magnificent job typing this report.

I am grateful to Iwan who provided me with a beautiful place to stay and to my roommate Tjien Hwie who often gave me a relaxing massage. I am also grateful to my friend Tung Bing for his company during my stay here at Caltech.

My fondest memory will always be with Fee Lan. Her understanding, kindness, care, and love has given me courage and strength especially when I am in despair and frustration. Furthermore, her delicious cooking keeps me healthy and strong.

Last but not least, I am deeply indebted to my family (in Indonesia) especially my mother, who nurtured me to be a decent gentleman, and provided me with continuing support which greatly contributed to the success of my education in the United States. Not to forget my sisters who provide good care and attention as well as regularly writing me letters. May God bless them in whatever they do.

ABSTRACT

Interest in accurate measurements of the time-dependent Poisson's ratio of polymers arises because it is a component commonly needed in stress analysis and it appears in most theories predicting the behavior of filled materials and composites. Because of the paucity of data and the difficulties in determining $\mu(t)$ experimentally, it has been customary in the past to treat $\mu(t)$ as a constant. This is unsatisfactory theoretically and inadequate for accurate work.

An apparatus has been constructed that enables us to measure tensile relaxation modulus, $E(t)$, and time-dependent Poisson's ratio, $\mu(t)$, *simultaneously* on the *same specimen* under the *same experimental condition*. The apparatus, which contains several novel features, is essentially in working condition. Experiments will be made on a series of selected polymers.

We hope to be able to determine the bulk relaxation modulus, $K(t)$, and the shear relaxation modulus, $G(t)$, from measurements of $E(t)$ and $\mu(t)$. A method for solving the appropriate convolution integrals to determine $K(t)$ and $G(t)$ is already available. It would be desirable to compare the calculated $G(t)$ and $K(t)$ with direct measurements. The latter are very difficult. Direct measurements of $G(t)$ will be made in a torsional relaxometer on the same specimen but not under identical conditions. Nevertheless, these data will be useful as a check on our measurements and our method of calculation.

This work will allow a comparison to be made between shear and bulk relaxation via the spectral functions. The measurements will ultimately form the basis for the development of a theory of bulk relaxation in polymeric materials.

TABLE OF CONTENTS

1. INTRODUCTION

The mechanical properties of a viscoelastic material are usually described by four functions of the time: the shear relaxation modulus, G(t), the tensile or Young's relaxation modulus, E(t), the bulk relaxation modulus, K(t), and the Poisson's ratio, $\mu(t)$. G(t) and K(t) relate to changes in shape and in size, respectively. The others may be considered to be derived moduli. For a homogeneous isotropic material, only two of these functions are needed to completely describe the viscoelastic properties of the material. The relationship between any three functions is obtained by replacing the elastic constants in the well-known elastic formulae (see Table 1) with the Carson transforms (i.e. the s-multiplied

Table 1

Relations Between the Elastic Constants

Elastic Constant	Expressed as function of:					
	G and E	G and μ	E and μ	K and E	K and μ	K and G
K	$\frac{GE}{9G - 3E}$	$\frac{2G(1 + \mu)}{3(1 - 2\mu)}$	$\frac{E}{3(1 - 2\mu)}$	-	-	-
G	-	-	$\frac{E}{2(1 + \mu)}$	$\frac{3KE}{9K - E}$	$\frac{3K(1 - 2\mu)}{2(1 + \mu)}$	-
E	-	$2G(1 + \mu)$	-	-	$3K(1 - 2\mu)$	$\frac{9KG}{3K + G}$
μ	$\frac{E}{2G} - 1$	-	-	$\frac{1}{2} - \frac{E}{6K}$	-	$\frac{3K - 2G}{6K + 2G}$

$\lambda = K - \frac{2}{3} G$ $\qquad$ $M = K + \frac{4}{3} G$

Laplace transform) of the time-dependent functions.

Instead of the time-dependent functions, the real and imaginary parts of the frequency-dependent functions $G^*(w)$, $E^*(w)$, $K^*(w)$, and $\mu^*(w)$ can be used.* The relationships between them is obtained by replacing the elastic constants with the complex quantities. These are applications of the so-called "Correspondence Principle". In the time-dependent mode inversion of the transform equations leads to convolution integrals (cf. Appendix C).

It is a well established fact that the shear and the tensile modulus are time-dependent[1]. The fact that the bulk modulus and the Poisson's ratio are also time-dependent is much less appreciated. In fact, they are often assumed to be time-independent constants. This report is concerned with the measurement of the time-dependent Poisson's ratio of viscoelastic materials in the transition region.

1.1 Earlier Determination of Poisson's Ratio

Measurements of Poission's ratio can be divided into four groups:

(1) Static measurements of the (time-independent) equilibrium Poisson's ratio, μ_e, and instantaneous or glassy Poisson's ratio, μ_g, on both anisotropic[2,3,4,5,6,7] and isotropic materials.[8,9,10,11]

(2) Time or temperature dependent measurements of Poisson's ratio on anisotropic materials.[12,13,14,15]

(3) Temperature dependent measurements of Poisson's ratio on homogeneous isotropic materials by:

(a) direct methods;[16] and

(b) indirect methods.[17,18,19]

(4) Time dependent measurements of Poisson's ratio on homogeneous isotropic materials by:

* w is used here for the circular frequency.

(a) direct methods;[20] and

(b) indirect methods.[21]

(5) Frequency dependent measurements of Poisson's ratio on homogeneous isotropic materials by:

(a) direct methods;[22,25,26,27,28,29] and

(b) indirect methods.[22,23,24,30,31,32,33,34]

Direct methods refer to the determination of Poisson's ratio from dimensional changes of the sample. Indirect methods refer to the determination of Poisson's ratio from knowledge of two other material functions, e.g. $E^*(w)$ and $G^*(w)$.

(1) Several techniques have been used to measure static Poisson's ratio Ward and Coworkers[6,7] have used interferometey, and following, by electron microscopy, the changes in spacings of a grid placed on the specimen. David[4] used optical diffraction. Fedors and Hong[11] used sensitive electric strain gauges. Fortuna et al.[10] used a simple dilatometric method to measure μ_e. None of these results will be discussed further here because we are interested in the time-dependent behavior.

(2) Richardson and Ward[15] used a Hall effect device to measure three of the Poisson's ratios on a low density polyethylene sheet with parallel lamellar morphology over a temperature range from +20°C to -60°C. Darlington and Saunders[12,13] used a differential capacitor linear displacement transducer to measure creep contraction ratios on an oriented low density polyethylene sheet. This device is attractive because it can measure the time-dependent tensile creep compliance and creep contraction ratio simultaneously. Again, further discussion of these results is outside the scope of our interest.

(3) The temperature dependence of the Poisson's ratio of homogeneous isotropic materials gives some qualitative insight into the behavior of the time-dependent Poisson's ratio in the transition region. Gilmour[16] et al. measured E(T) and $\mu(T)$ using bidirectional strain gages on polystyrene, poly(methyl methacrylate) and polycarbonate in the glassy state. Crowson and Arridge[18,19] measured the temperature dependence of the shear compliance, J(t), and the bulk compliance B(t), on epoxy resin polymers. They calculated $\mu(T)$ from the relations

$$D(T) = \frac{3B(T) + J(T)}{9B(T)J(T)} \tag{1}$$

$$\mu_{DJ}(T) = 2\,\frac{J(T)}{D(T)} - 1 \tag{2}$$

and showed that small systematic errors in the temperature measurements can lead to maxima cr minima in the calculated $\mu(T)$. The best available temperature dependent data were obtained by Waterman.[17] He used an ultrasonic pulse method to determine the complex tensile, shear, and bulk moduli of isotactic polypropylene and various polyethylenes. The temperature ranged from -90°C to 140°C at a constant frequency of 5 MHz. The complex Poisson's ratio was calculated. No minima were obtained. Waterman also showed that both the γ and the β transitions in polyethylene cause dispersion in the bulk modulus as well as in the Poisson's ratio. For isotactic polypropylene the peak in tan δ (the ratio of the imaginary to the real component) of the bulk modulus is not the same as for shear modulus, as expected from theory.

(4) The time-dependent Poisson's ratio, $\mu(t)$, has not been measured directly. Philip Chan[20] tried to measure $\mu(t)$ using photographic techniques and a Hall effect device but failed because of lack of resolution. The indirect method was used by Theocaris[21] who measured the tensile creep compliance, D(t), and the tensile relaxation modulus, E(t), of pure cold-setting epoxy polymers over the whole transition region. He calculated Poisson's ratio from D(t) and B(t) as $\mu_c(t)$, and from E(t) and K(t) as $\mu_r(t)$ using an approximation based on the fact that the bulk compliance and bulk modulus of viscoelastic materials are fairly insensitive functions of time. Knowing E(t), D(t), $\mu_c(t)$ and $\mu_r(t)$, B(t) and J(t), as well as K(t) and G(t) were calculated. Unfortunately, some of the formulae he used were incorrectly derived. Consequently, $\mu_c(t)$ and $\mu_r(t)$ differed, particularly in the transition region. Theoretically, both functions must be the same, and the error may have been exaggerated by the approximation method he used. Since the values of $\mu_c(t)$ and $\mu_r(t)$ were incorrect, the other functions (G(t), K(t), J(t), B(t)) calculated from these values were not correct either.

(5) More studies have been made in the frequency dependent mode. The frequency-dependent Poisson's ratio may be derived from the other complex functions by the equation

$$\mu^*(w) = \frac{E^*(w)}{2G^*(w)} - 1 = \tfrac{1}{2} - \frac{E^*(w)}{6K^*(w)} = \frac{3K^*(w) - 2G^*(w)}{6K^*(w) + 2G^*(w)} \qquad (3)$$

Philippoff and Brodnyan[30] measured $E^*(w)$, $G^*(w)$, and the real component of $K^*(w)$, i.e. $K'(w)$, over the range from 3×10^{-4} to 5Hz and -25° to 95°C on plasticized poly (vinyl chloride). Each function was measured separately. They were not able to measure the imaginary

component, K''(w), satisfactorily. They obtained μ*(w) from E*(w) and G*(w). A minimum was observed in the real part of μ*(w). They also obtained a constant value for μ'(w) when this was calculated from $\frac{1}{2}$ - E'(w)/6K'(w) which is, of course, wrong. Speculations of Koppelmann[31,32,33] concerning the behavior of Poisson's ratio in the transition region based on measurements of E*(w), G*(w), and M* = K*(w) + (4/3) G*(w) may be summarized as implying that minima observed when μ*(w) is calculated from complex moduli, may be due either to inadequate temperature control (cf. Arridge and Crowson[18,19]), or to the fact that the elastic relationships between the moduli do not hold in the transition region. This is, of course, perfectly true. However, minima which are contrary to the predictions of linear viscoelasticity seem to appear whenever the frequency dependent Poisson's ratio is calculated from measurements of complex moduli. Clearly, highly accurate data are needed. Generally the calculations are based on measurements in which the two complex moduli were made on different test specimens. This is bound to affect the accuracy of the data adversely.

Heydemann and coworkers [23,24] measured E*(w) and G*(w) on the same plasticized poly(vinyl chloride) over a frequency range from 50 to 1000 Hz at temperatures ranging from -80 to +100°C. Using these data, Heydemann[22] calculated μ*(w) and again found a minimum in μ'(w) as a function of temperature at constant frequency. When μ'(T) (at 1 kHz) was calculated by the same author[22] from new, more accurate data obtained at lower rates of temperature change, no minimum was found. Direct measurements of μ'(T) at 4 Hz also did not reveal any minimum.

Thomson[34] also calculated μ*(w) from E*(w) and G*(w) obtained on a urethane rubber compound. The data were taken on different samples, and were measured in different apparatus by different persons. His results are

totally inconsistent with theory: he observed both a minimum and a maximum.

The most comprehensive study of Poisson's ratio is that by Yee and Takemori[26,27,28,29] who measured $\mu^*(w)$ and $E^*(w)$ simultaneously. They used a servohydraulic tester to apply a small oscillating tensile strain and measured the longitudinal and transverse strains by the use of appropriately placed extensometers. From $\mu^*(w)$ and $E^*(w)$ they then obtained $G^*(w)$ and $K^*(w)$. Their study is concerned primarily with the glassy region and does not provide insight in the behavior of the components of $\mu^*(w)$ in the transition region.

The only data obtained as a function of frequency in the transition region are those of Kästner and Pohl.[25] They measured $E^*(w)$, $G^*(w)$, and $\mu'(w)$. $K'(w)$ was calculated from these measurements. They found $\mu''(w)$ to be too small to be measured. No minimum appeared in $\mu'(w)$. Again, the different measurements were made on different specimens using different instruments. A detailed analysis of their data is presented in Appendix A. It was not possible to obtain $\mu'(w)$ by calculation.

1.2 Considerations Relating to the Development of a New Experimental Procedure.

The viscoelastic theory of the time (or, equivalently, the frequency) dependent Poisson's ratio is outlined in Appendix B. The theory requires that the complex ratio be expressed in terms of its real and imaginary parts by

$$\mu^*(w) = \mu'(w) - j\mu''(w) \tag{4}$$

Many authors erroneously link the components by a plus sign.[26,34,35]

From $E^*(w)$ and $G^*(w)$, the components of $\mu^*(w)$ are obtained by

$$\mu'(w) = \frac{E'(w)G'(w) + E''(w)G''(w)}{2\tilde{G}^2(w)} - 1 \tag{5}$$

and

$$\mu''(w) = \frac{E'(w)G''(w) - E''(w)G'(w)}{2\tilde{G}^2(w)} \tag{6}$$

where $\tilde{G}^2(w) = [G'(w)]^2 + [G''(w)]^2$. The need for very accurate primary data is obvious.

If at all possible, Poisson's ratio should be measured directly. It is clear that inaccuracies in the data resulting from differences in the geometry (end effects)and/or the material properties of the test specimens can foil any attempt to calculate the ratio from measurements of moduli or compliances. In this connection it is interesting to quote the modelling attempts of Gothenberg and Christensen[35] who, although they used the wrong form of Eq. (4), showed that even quite small changes in the parameters of the model can have profound effects on the shape of the calculated curves, producing minima inconsistent with theory.

Once the decision is made to measure Poisson's ratio directly, the question arises whether the measurements should be made in the frequency or the time-dependent mode. There is sufficient evidence that $\mu''(w)$ is exceedingly difficult to measure.[22,25] On that score alone, time-dependent measurements would appear to be preferable.

The earlier work just cited has often emphasized the need for exacting temperature control. It would appear that a liquid control bath surrounding the specimen is mandatory to achieve a halfways adequate control of temperature. This again argues against a frequency dependent mode of measurement because of the disturbing effects of oscillations of the bath liquid. A liquid bath poses problems also in that the specimen may swell. A suitable bath liquid (such as silicone or fluorocarbon for

measurements on hydrocarbon polymers) must be found. The problem of Poisson's ratio and the tensile modulus in a swollen specimen has been considered by Kuhn [44] and might provide means for correction.

The possibility of measuring Poisson's ratio and Young's modulus simultaneously on the same test piece under identical experimental conditions opens the way for a possible determination of the time-dependent bulk modulus, K(t), from these measurements. As shown in Appendix C, this requires the solution of convolution integrals. The necessary equations, using the method of Hopkins and Hamming[37], have been developed by Cronshaw[36] who has also written and tested out computer programs for the numerical work.

The time-dependent bulk modulus, just as the time-dependent Poisson's ratio, has received relatively little attention compared to the time-dependent tensile and shear moduli. The current state of our knowledge concerning bulk relaxation in polymeric materials has been reviewed, e.g. by Marvin and McKinney[39], by Ferry,[1] and by Yee and Takemori.[29] Techniques for measuring bulk relaxation have also been reviewed, e.g. by Ferry.[1] They can again be grouped into the broad classes of direct and indirect measurements. Direct measurements aim to determine volume changes resulting from changes in pressure in essentially the same way in which length changes resulting from changes in tension are determined, except that the experimental difficulty inherent in volume-pressure measurements are at least an order of magnitude greater.

Most of the work has been done in the frequency dependent mode using both direct and indirect measurements. The best work may have been done by Marvin, McKinney and co-workers[40,41,42,43] using a direct measurement technique and by Yee and Takemori[29] using an indirect one.

Little work has been done in the time-dependent mode. Crowson and Arridge[18] measured the time-dependent bulk compliance, B(t). The data of Theocaris[21] are, unfortunately, flawed.

2. APPARATUS

As mentioned above, practically no usable data appear to exist on $\mu(t)$. Experimentally, measurement of the time-dependent Poisson's ratio has been hampered by the fact that it requires the detection of very minute changes in the specimen thickness (height). By definition,

$$\mu(t) = -\varepsilon_2(t)/\varepsilon_1 = -[\Delta h(t)/h_o]/[\Delta \ell/\ell_o] \tag{7}$$

where ε_1 is the strain applied to the specimen, $\varepsilon_2(t)$ is the lateral contraction in the direction perpendicular to the direction of the strain imposed on the specimen, $\Delta h(t)$ is the change in height, $\Delta \ell$ is the length change, and h_o and ℓ_o are the inital height and length, respectively. The difficulty lies particularly in determining the thickness changes. We attempt to achieve this by the use of an ultrasensitive detector.

As will be shown in the next section, we must be able to detect thickness changes of at least 0.1 μm. Polymer specimens cannot be fashioned to this degree of tolerance. Hence, it is necessary to observe the changes in the same location, uneffected by the deformation (stretch) of the specimen.

Equally obvious is the need for exacting temperature control. Considering a 3-mm-thick specimen with a linear expansion coefficient of 2×10^{-4} reciprocal degrees, one degree change in temperature will cause a thickness change of 0.6 μm. Thus, the temperature must be kept constant within at least ± 0.01°C.

The apparatus designed to allow us to measure the time-dependent Poisson's ratio, $\mu(t)$, simultaneously with the tensile modulus, $E(t)$, has been constructed and is essentially in working order. The design of the apparatus enables us to determine the thickness of the specimen (i.e. the lateral contraction) in the same location, unaffected by the deformation of the specimen. This is an important feature of the new method and is expected to enhance the precision of the measurements. A perspective drawing of the apparatus is shown below.

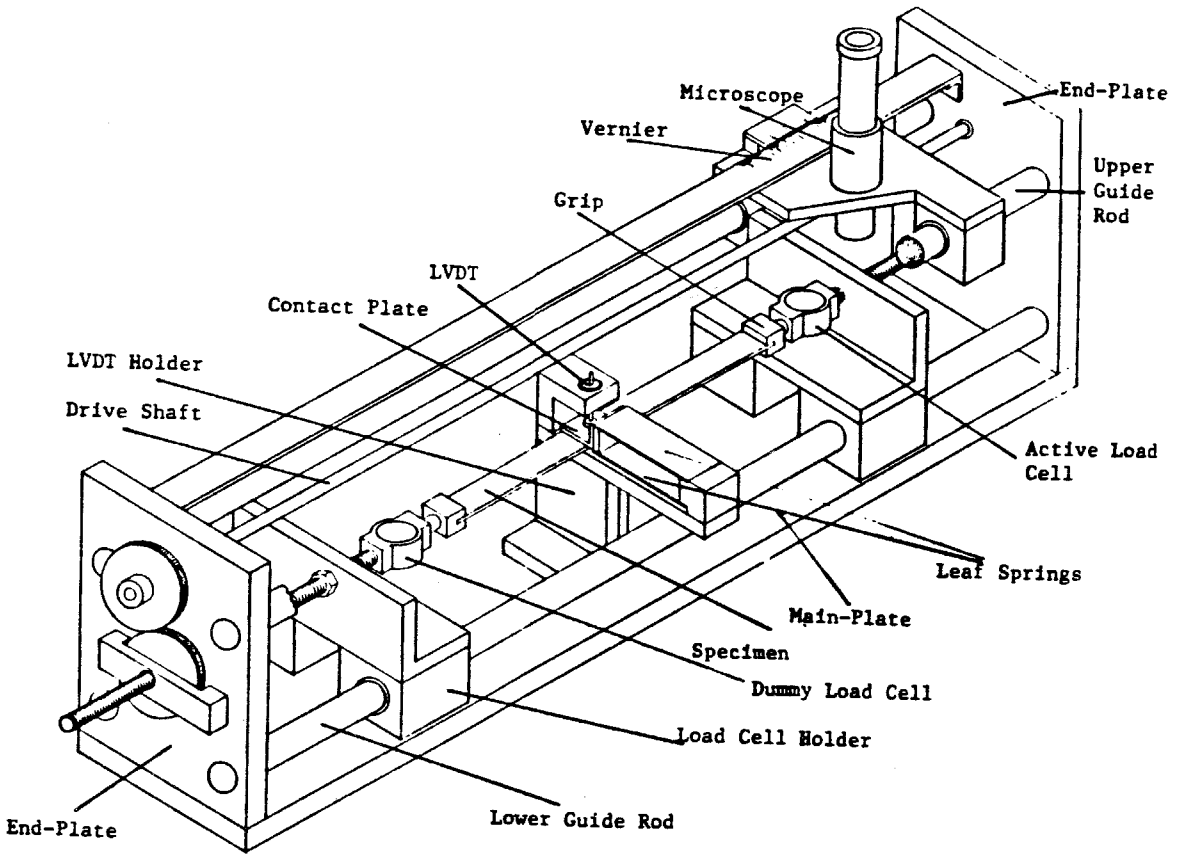

Fig. 1. Stretching device for measuring Poisson's ratio.

The various parts of the apparatus are mounted on a main-plate between two end plates which are connected by two lower and two upper guide rods. They were cadmium plated for protection against corrosion. The specimen, a strip of rubber about 12-cm-long and 1-cm-wide, is attached by grips at one end to an active, and at the other end to a dummy load cell. The load cell holders slide on the lower guide rods and can be driven in opposite directions through drive shafts and gears. A variable-speed Bodine motor and gear box (not shown) provides the drive. A micro-switch assembly, which is part of the drive mechanism, confines the travel of the load cell holders within appropriate limits at all times.

2.1 Load Cells

The tensile stress is measured by the active load cell. The dummy load cell ensures that the compliance is the same on both sides of the specimen so that when it is stretched, both halves extend evenly and at the same rate. There is thus a neutral line in the center of the specimen where the motion is zero.

Three ESA active load cells (of 10, 100, and 1000 lb capacity) have been obtained from Saber Enterprises, Long Beach, California. They are fitted with Micro-Measurement strain gages. The dummy load cells are identical in construction but carry no gages. A 12 volt car battery is used to provide a D.C. input voltage to the load cell. The load cell signal is fed into the first channel of the electronic switch (see Section 2.3) from whence it proceeds to a chart recorder. The position of the load cells and of the specimen grips attached to them is critical. They must be at the same height and must be parallel to each other to prevent twisting of the specimen.

2.2 Thickness Sensor

The changes in the thickness of the specimen are measured with the aid of a highly sensitive Schaevitz Model MHR 005 temperature compensated linear variable differential transformer (LVDT) which has the required resolution (see Section 3.2). The carrier frequency of 10 kHz is supplied from a Schaevitz Model CAS 100 signal conditioner which also demodulates and amplifies the voltage generated in the secondary windings. The correct operating voltage in the primary is 3.5 VRMS. The gain could be increased by increasing this voltage (5 VRMS maximum). However, this was found to generate too much heat in the windings and tended to cause the output signal to drift.

Some of the 10 kHz carrier frequency leaks to the output of the LVDT. Even though the LVDT is temperature compensated, the signal conditioner is not. The LVDT output signal varies when the signal conditioner's temperature varies. In order to keep the signal conditioner at a reasonably constant temperature, it is kept covered at all times by a wooden hood.

The LVDT has a linear range of ±0.127 mm (0.005 in.). To measure the thickness changes correctly, the LVDT core must be located in the linear region. Every time a new specimen is used, the core position must be rechecked to assure that is lies in the linear region.

The output from the signal conditioner is fed to the second channel of the electronic switch (see Section 2.3). The primary connections on the CAS were reversed to obtain an increase in the output signal for a decrease in specimen thickness.

The alignment of the LVDT coils with respect to the core is crucial. They cannot touch the core at any time. The coils are positioned with a

set of setscrews in the LVDT holder. This is constructed in such a manner that that part of it (called the table) which is in contact with the underside of the specimen can be adjusted vertically to ensure proper seating of the specimen. It can also be displaced along the long axis of the stretching device to locate it exactly over the neutral line. Details of the latter two mechanisms are omitted from the drawing for clarity. The holder is positioned with the help of a Gaertner Scientific Co. travelling microscope and a Vernier scale which are also used to determine the elongation of the specimen.

The rod bearing the core is attached to a contact plate suspended from two parallel 0.127 mm (0.005 in.) thick phosphor bronze leaf springs. These prevent any but up-down travel of the rod. They must be aligned precisely so that the contact plate and the table remain parallel at all times. This can be checked by sliding a parallel copper dish between the plate and the table and monitoring the LVDT output. The output should not change by more than 3 mV when the dish is moved around.

Some experiments were made to find the most suitable contact area. Point contact, circular contact areas of 0.140, 0.187, and 0.250 in. diameter, and rectangular contact areas of 0.0625, 0.125, 0.250, 0.500, and 1.000 in. by 2 in. were tried. Only the 0.250, 0.500, and 1.000 in. wide rectangular plates gave satisfactory output. Further experiments showed that the 0.500 in. plate produces the best output.

There appears to be considerable adhesion between the contact plate and the specimen because of a thin layer of silicone oil between them. With a sufficiently large area, this force will keep the specimen and the plate in contact at all times. Stick-slip during stretching was successfully eliminated by Teflon cladding the table as well as the contact plate.

The suspension system consisting of the leaf springs, the contact plate, and the LVDT rod-and-core was kept as light as possible to prevent undue compression of the specimen. When immersed in the silicone bath oil, the system constitutes a damped pendulum. Its damping characteristics were measured. It was decided that, over the range of thickness change encountered in the delayed contraction of the specimen, the damping of the motion of the suspension could be neglected, particularly since the adhesive force tends to drag it along.

2.3 Electronic Switch

To enable us to detect small changes in the LVDT and load cell outputs a sophisticated electronic switch has been constructed. This switch, which has a variable gain from 1 to 100 in each of two channels, allows both output signals to be changed in character at the moment that the specimen has reached its predetermined elongation (at time t'). At this moment the signals are off-set back to the bottom of the pen recorder chart, the load cell signal (but not the LVDT signal) is reversed and the amplification is increased simultaneously. The voltage appearing at that moment across the terminals of each channel is recorded accurately in two LED displays in terms of calibrated counts.

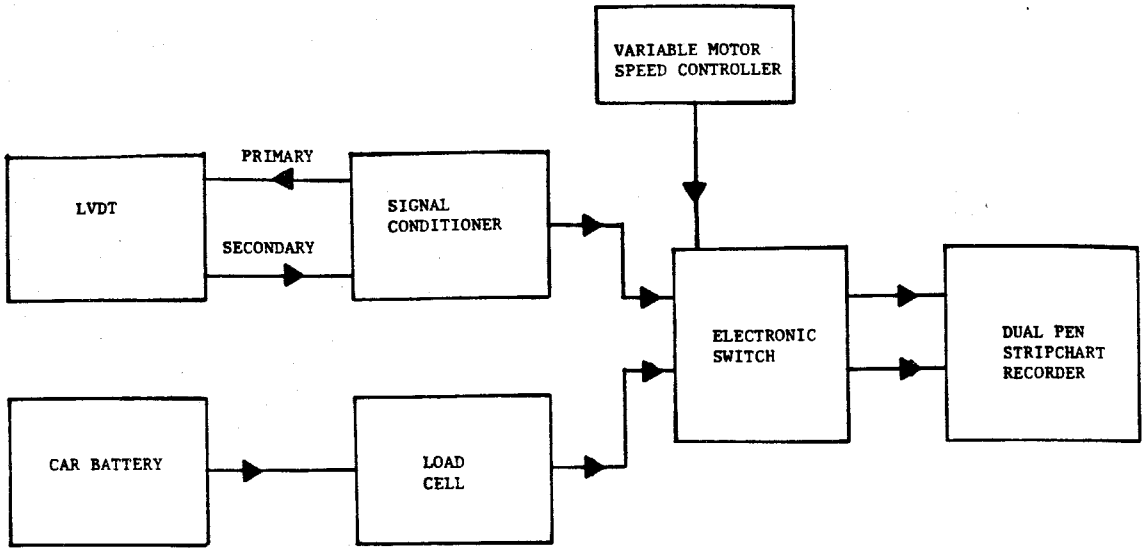

Fig. 2. Block Diagram of Electronic Components

Figure 2 shows the position of the switch among the various components of the apparatus. Circuit and wiring diagrams are assembled in Appendix E. Figure 3 illustrates the working of the switch. It is crucial to the success

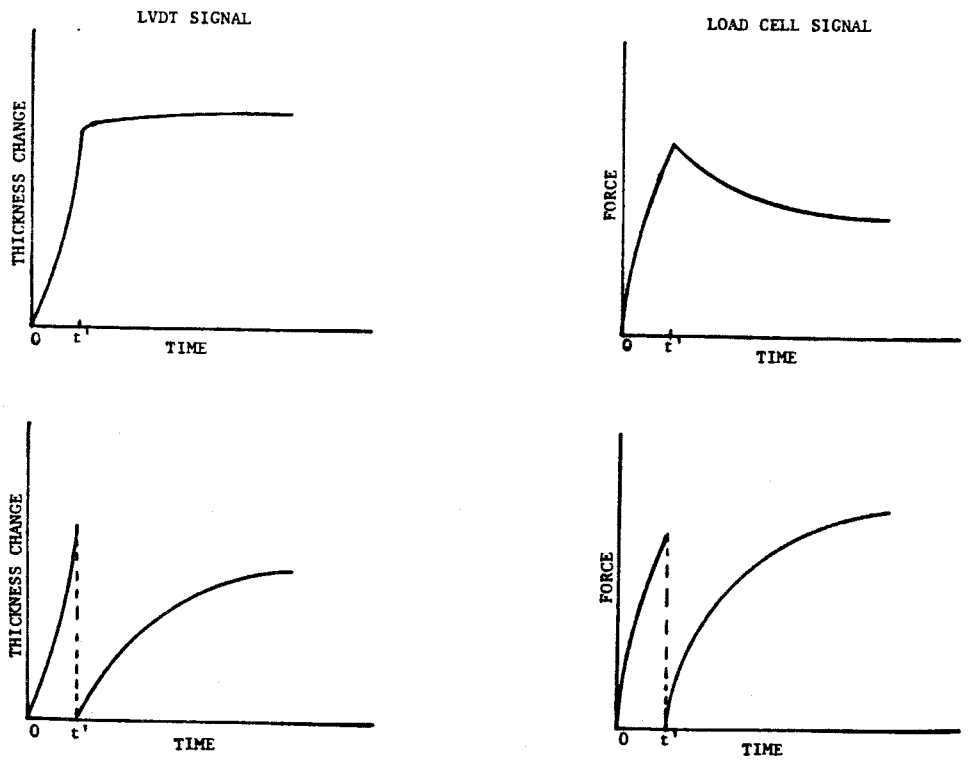

Figure 3. Electronic signals: (a) upper portion, as received by electronic switch; (b) lower portion, emanating from electronic switch.

of our measurements and is ultimately responsible for allowing us to achieve the required resolution.

The switch responds to positive signals only. It is designed for a maximum input of 3.8 V in the LVDT-channel, and 15 mV in the LC-channel. The offset voltage is 9.31×10^{-4} V per digital count in the former, and 3.67×10^{-6} V per digital count in the latter channel. Accurate knowledge of the displayed voltages allows precise calibration of the signal traces appearing on the pen recorder chart.

Initial problems experienced with the switch came from the fact that its analog to digital converters are very sensitive to noise. Noise from the LVDT signal comes from the 10 kHz carrier frequency. This was eliminated by putting a low-pass filter in the circuit. The remaining low frequency noise does not pose any problem since its peak magnitude is only ±0.1 mV and we measure about 1 volt changes in LVDT output. This noise level therefore produces only one error count in the offset voltage.

The problem is more difficult with the load cell because of the less favorable signal-to-noise ratio. Originally, a Hewlett Packard 6218A power supply was used to provide the 10 volt input voltage for the load cell. The power supply produces about 3 mV of 60 Hz noise. This noise is significant because we measure about 1 to 2 mV change in the load cell output. A high-pass filter significantly depressed the output signal. The solution was a 12 volt car battery with a rheostat to regulate the input voltage. The noise was eventually reduced to 8 μV by shielding all cable connections and surrounding the car battery with a Faraday cage.

The electronic switch is activated when the switch on the motor controller for the Bodine motor is thrown into brake position. However, at this instant the specimen is still being stretched because the

response cannot be instantaneous. The delay is about 0.1 second. An adjustable delay circuit has been installed in the variable motor controller. The delay circuit is set by displaying simultaneously on the two-channel recorder the signal from the electronic switch and the same signal taken directly from the load cell. By comparing the two signals the circuit is adjusted until the switching time of the electronic switch is suitably delayed. The switch becomes activated only when the motion of the grips has stopped.

2.4 Temperature Control

To ensure proper temperature control during measurements, the stretcher is placed into an aluminum tank filled with Dow Corning 200, 10 centistokes silicone oil, up to just above the upper guide rods. To prevent water condensation, the tank will be completely sealed from air circulation. The tank, which acts as a large heat capacitor, is placed into a well insulated environmental chamber connected to a Missimers Temperature Servo which produces a flow of conditioned air around the tank. The temperature ranges from -40°C to 175°C and with the help of liquid nitrogen can reach -100°C. It is regulated by a Hallikainen Thermotrol proportional controller. A sensitive resistance thermometer manufactured by Temtech, Inc., senses the temperature in the environmental chamber. The maximum air temperature fluctuation is ±0.15°C. In the tank this is reduced to ±0.01°C. There is some temperature difference between the edge and middle of the tank (less than 0.1°C); however, this does not concern us since the temperature near the specimen varies only by ±0.01°C. The LVDT and load cell output signals are practically constant under temperature fluctuations of this magnitude.

The temperatures both of the environmental air flow and of the bath liquid are continuously monitored by thermocouples whose output is displayed on a second two-pen chart recorder. In the bath, the thermocouple is placed near the contact plate. To check the temperature fluctuation in the bath, the thermocouple output is amplified by passing it through the LC-channel of the electronic switch.

3. CALIBRATION

The output signals from the load cell (LC) must be calibrated in terms of force. That from the LVDT requires calibration in terms of displacement (thickness change).

Since both the LC and the LVDT are immersed in the temperature bath, the output signals must be calibrated as functions of temperature.

3.1 The Load Cells

Only the 10-lb and the 100-lb load cells were calibrated at this time. The cells were suspended in the environmental chamber of an Instron Tester and their output was determined as function of temperature and of the known calibration weights attached to them. The voltage output was measured using a Fluke Model 8800A digital voltmeter which is capable of measuring voltage down to 1 μV.

For the 10-lb cell the force is then obtained from

$$f = D(T)[V-V_o(T)] + E(T)[V-V_o(T)]^2 \qquad (8)$$

where V is the output in mV's,

$$D(T) = 1.066\times10^{-2}T + 69.070 \qquad N/(mV) \tag{9}$$

$$E(T) = 8.9752\times10^{-4}T + 5.435\times10^{-2} \qquad N/(mV)^2 \tag{10}$$

and

$$V_o(T) = 1.742\times10^{-3}T + 0.504 \qquad mV \tag{11}$$

The temperature is in degrees Celsius. The dependence of D and E on temperature is shown in Figure 4. The fit is excellent for D(T). There is more scatter in E(T) but the quadratic term only represents a correction of the second order. Repeated measurements showed the errors to be less than 0.2%. The maximum error was 0.5%.

The force-voltage relationship for the 10-lb cell is simpler because the temperature dependence of D and E could be neglected within the required accuracy. We have

$$f = 10.545\ [V-V_o(T)] + 3.327\times10^{-2}\ [V-V_o(T)]^2 \tag{12}$$

where

$$V_o(T) = 2.073\times10^{-3}T + 0.7208 \qquad mV \tag{13}$$

In view of the smaller forces, the errors are typically less than 0.5% with a maximum error of 1%.

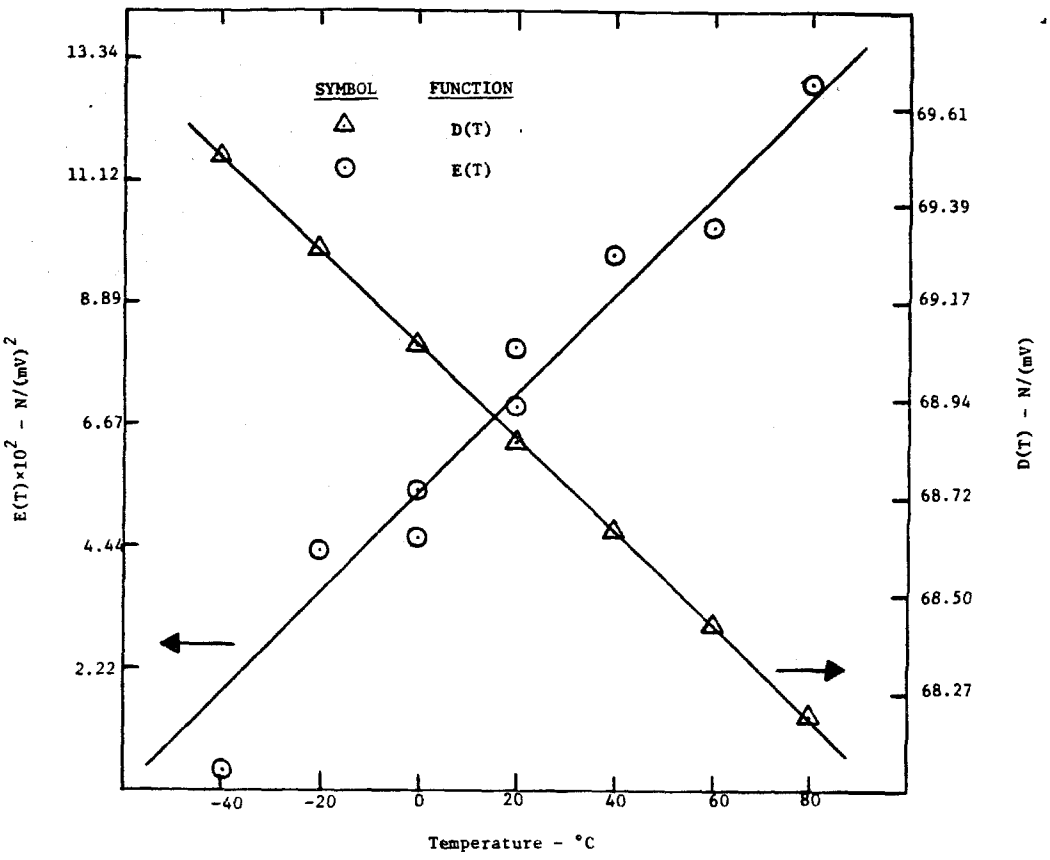

Figure 4: Calibration curve for 100 lb load cell as function of temperature.

The calibration was checked satisfactorily on a test sample. This was a styrene-butadiene block copolymer of unknown composition having a relatively high glass transition temperature. Thus the sample relaxed noticeably at room temperature. The relaxation modulus determined in the stretcher is compared with that obtained in the Instron tester in Figure 5. The agreement is excellent, except at times shorter than about one minute. This deviation undoubtedly arises from differences in the "ramp time" (1.50 and 0.08 seconds, respectively) required to reach the ultimate elongations of 4.9% (stretcher) and 3.2% (Instron). Even so, the maximum deviation at these short times was only 2%.

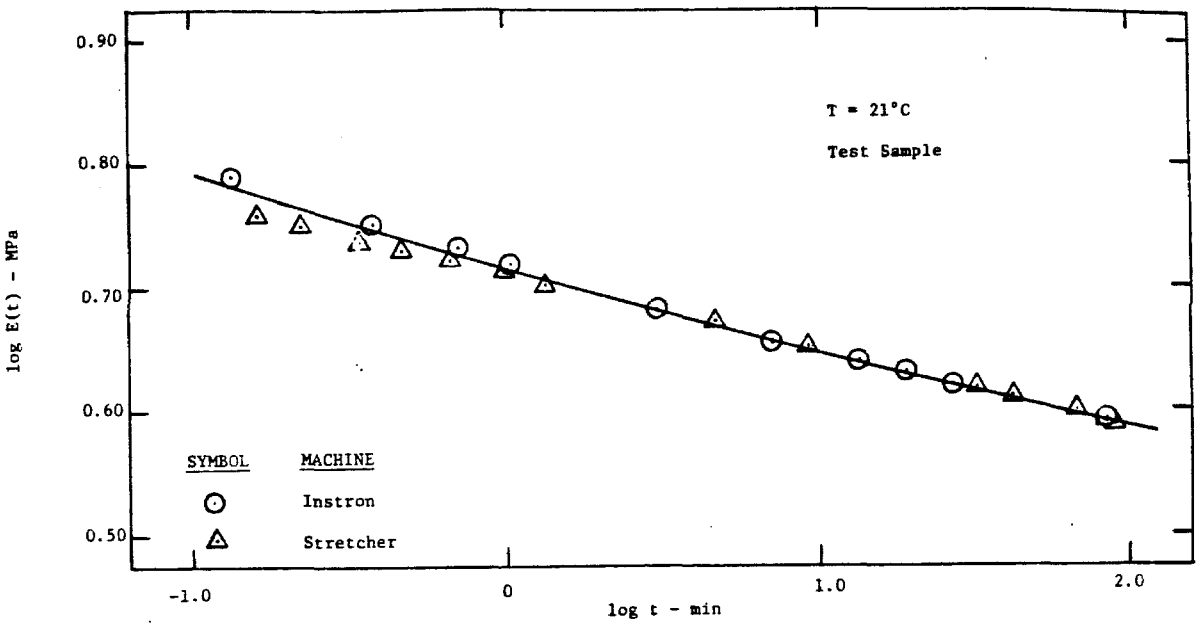

Figure 5: Stress relaxation of test sample measured in the Instron tester and the stretcher, respectively.

3.2 The LVDT

For exploratory measurements around room temperature the LVDT was calibrated using a micrometer accurate to 2.5 μm. In this case

$$\Delta h = C(T)\Delta V \tag{14}$$

where Δh is the change in height (thickness) of the specimen, C(T) is the gain and ΔV is the difference in voltage output. For work around room temperature C can be considered to be a constant. The magnitude of C can be varied in the signal conditioner. The maximum value is close to 83.3×10^{-6} m/V. This is equivalent to an output of 12 mV for a 1 μm change in thickness which could easily be seen on our chart recorder whose maximum sensitivity is 1 mV full scale. The thickness change on

stretching is about 25-50 μm. Thus the chart recorder is set typically to 1 V full scale (i.e. about 83 μm full scale). When the specimen has attained the desired elongation, the electronic switch is activated. The 100-fold gain in the switch now allows for about 0.83 μm full scale on the chart. Calculations of Chan[20] showed that we need to be able to detect thickness changes of about 0.1 μm in the glassy and equilibrium regions and about 2 μm in the center of the transition region at 1% strain. Since we are not interested in secondary transitions in the glassy region, a strain of 1% should be tolerable and the resultant output should be just within the capability of the instrument. As we proceed through the transition region to the equilibrium response, the strain can be increased if required (particularly in the rubbery region). Thus it appears that the expected thickness changes should be detectable with just enough accuracy.

Overlap of isothermal segments should further help in defining the master curve. Recording of the isothermal segments at different temperatures requires calibration of the LVDT as a function of temperature. This to be accomplished with accurately machined disks of high purity copper[45] with known coefficient of expansion. The procedure for doing this (including computer programs) have been worked out by Moonan.[46] With the LVDT currently employed, the calibration depends on the thickness of the specimen. We expect to purchase another LVDT with an extended linear range. This will considerably simplify the calibration for temperature dependence.

4. EXPERIMENTAL RESULTS

An attempt was made to measure the time-dependent Poisson's ratio on a styrene-butadiene rubber (SBR). Because of the low glass transition temperature of this sample ($\sim$ -57°C), covering the transition region requires working at low temperatures. Below -10°C we experienced considerable trouble because of water condensation when the bath returned to room temperature. These experiments therefore had to be deferred until the bath could be provided with a hermetically sealed cover and a dry nitrogen or dry air blanket. Currently, a special sample of styrene-butadiene rubber having a high styrene content ($\sim$ 63%) is being prepared for us by courtesy of Firestone Tire and Rubber Company. The glass transition temperature of this sample will be well above room temperature. This will allow us to make measurements in a comfortable temperature range pending the redesign of the tank.

Some interesting information was obtained from experiments on a sample of a styrene-butadiene block copolymer of undisclosed composition. This sample evinced considerable relaxation at room temperature. Figure 6 shows both $E(t)$ and $\mu(t)$. The Poisson's ratio is quite high. This does not appear to be an artifact because the random SBR gave Poisson's ratio close to 0.5 at room temperature. We believe that the high values of $\mu(t)$ recorded on the block copolymer could result from strain induced anisotropy. Such anisotropy[48] can produce E to G ratios well in excess of 3, the theoretical value for a homogeneous isotropic rubber. By the relation

$$\mu = E/2G - 1 \tag{15}$$

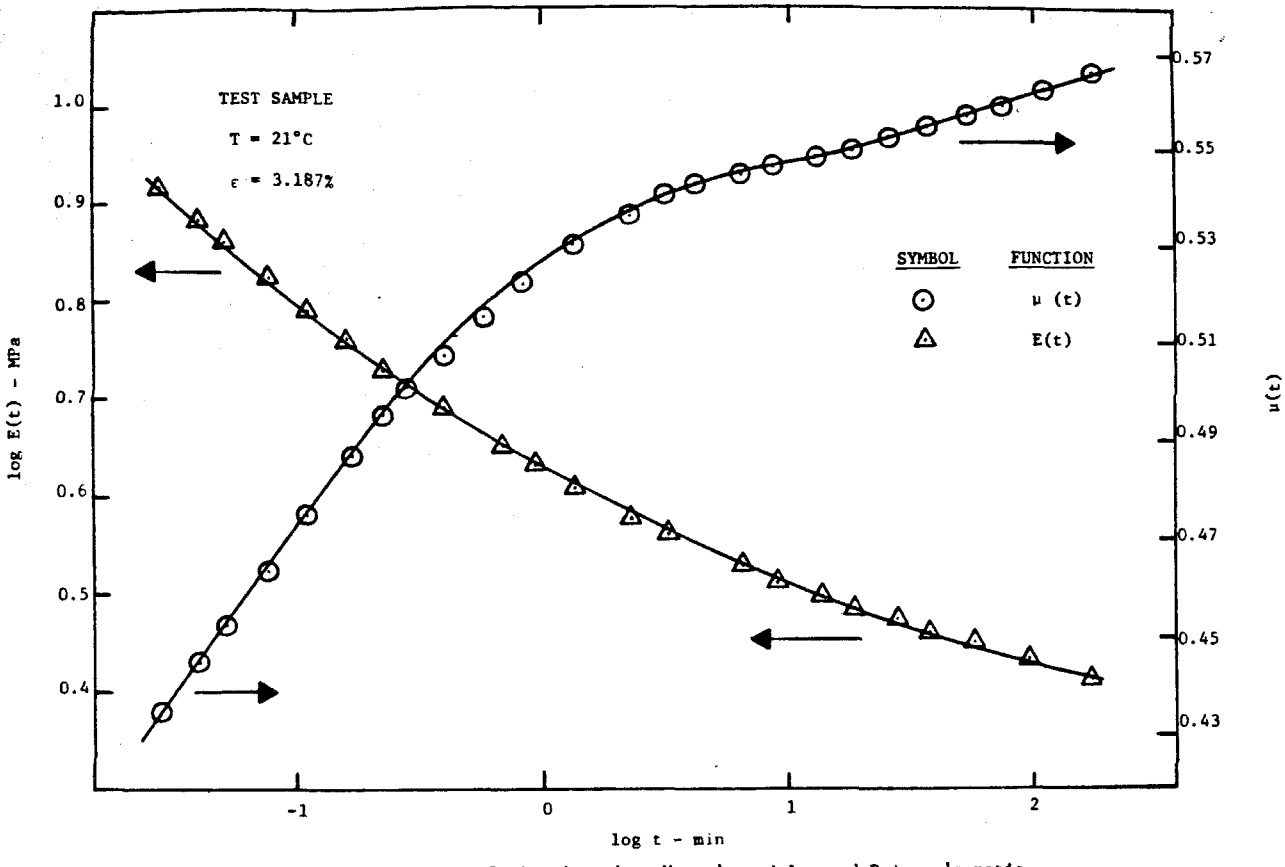

Figure 6: Simultaneous measurement of time dependent Young's modulus and Poisson's ratio.

(see Table 1), an E to G ratio of 3.2 yields a Poisson's ratio of 0.6. It appears likely that much interesting information could be obtained from studying the Poisson's ratio of block copolymers as a function of stretch and of composition. It is noteworthy that $\mu(t)$ clearly shows an inflection around 15 minutes which is just barely noticeable in E(t).

5. FUTURE WORK

Figure 6 demonstrates the capability of our instrument. It still remains, however, to obtain a full record on a well characterized sample. We hope to be able to produce this when the Firestone sample becomes available.

Some improvements in the instrumentation and the experimental procedure need to be made. A new LVDT with a longer linear range is now available and would greatly ease calibration problems. We shall need some device (such as, for instance, a travelling potentiometer) to allow us to determine grip separation inside the closed environmental chamber. Our method for determining the initial thickness of the specimen needs to be sharpened. Currently, we measure h_o before installation of the specimen with a dial gage having an accuracy of 0.001 in. We are exploring methods to make an absolute calibration of the LVDT *in situ* with greatly improved accuracy.

Swelling of the specimen in the bath liquid is a potential source of error. We found that SBR will swell in silicone oil upon prolonged exposure. The swelling is difficult to detect by weighing but can be seen between crossed polarizers. We think that no noticeable swelling will occur over the time required for an experimental run. Experiments to check this are currently under way. We are also investigating the use of different bath liquids such as, for instance, fluorocarbons. In the worst case, a correction could be made using the equation of Kuhn[44] according to which the unswollen Poisson's ratio is

$$\mu = \mu_{sw} + 1.5 - 1.5\, E_{sw}/E \tag{16}$$

where the subscript sw refers to measurements on the swollen sample. The correction essentially entails separate measurements of E(t) in air.

Once the remaining experimental problems have been dealt with, we wish to undertake a systematic of Poisson's ratio on several amorphous, non-crystallyzing polymers in the main transition region. We should be

able to make measurements not only on SBR, NBR, possibly urethane rubbers and others, but also on PMMA and PS. As pointed out in Section 4, investigation of block copolymers could be richly rewarding.

When successful measurements have been obtained on at least one sample, we shall explore the possibility of calculating G(t) and/or K(t) from our measurements of E(t) and μ(t). We intend to make measurements of G(t) on our torsional relaxometer to check the validity of the methods outlined in Appendix C. Relaxation spectra will be calculated and compared.

It is expected that these studies will contribute significantly to our understanding of relaxation phenomena in polymeric materials.

REFERENCES

1. Ferry, J.D., *Viscoelastic Properties of Polymers*, 2nd ed., Wiley and Sons, New York, (1970).

2. Holownia, B.P., Rubber Chem. Tech., 48, 246 (1975).

3. Frank, F.I., and Ruoff, A.L., Text. Res. J., 28, 213, (1958).

4. Davis, V., J. Text. Inst., 50, 1688 (1960).

5. Ladizesky, N.H., and Ward, I.M., J. Macromol. Sci. Phys., B5(4), 661 (1971).

6. Wilson, I., Cunningham, A., and Ward, I.M., J. Mat. Sci., 11, 2181 (1976).

7. Wilson, I., Ladizesky, N.H., and Ward, I.M., J. Mat Sci., 11, 2177 (1976).

8. Lethersich, W., J. Sci. Ins., 21, 180 (1944).

9. Lobdell, A.J., Shinopulos, G.F., and Fileo, D.N., Material Research and Standards, 4, 8 (1964).

10. Laufer, Z., Diamant, Y., Gill, M., and Fortuna, G., Int. J. Polym. Mat., 6, 159 (1978).

11. Fedors, R.F., and Hong, S.D., J. Polym. Sci., Polym. Phys. Ed., 20, 777 (1982).

12. Darlington, M.W., and Saunders, D.W., J. Phys. D3, 535 (1970).

13. Darlington, M.W., and Saunders, D.W., J. Phys. E3, 511 (1970).

14. Clayton, D., Darlington, M.W., and Hall, M.M., J. Phys., E6, 218 (1973).

15. Richardson, I.D., and Ward, I.M., Polym. Phys. Ed., 16, 667 (1978).

16. Gilmour, I.W., Trainor, A., and Howard, R.N., J. App. Polym. Sci. 23, 3129 (1979).

17. Waterman, H.A., Kolloid-Z. Z-Polym., 192, 1 (1963).

18. Crowson, R.J., and Arridge, R.G.C., Polymer, 20, 737 (1979).

19. Crowson, R.J., and Arridge, R.G.C., Polymer, 20, 747 (1979).

20. Chan, P., *A Study to Determine the Feasibility of Measuring the Time-Dependent Poisson's Ratio in Rubbers*, Master Report, California Institute of Technology, Pasadena, (1978).

21. Theocaris, P.S., J. Mech. Phys. Solids., 12, 125 (1964).

22. Heydemann, P., Kolloid-Z. Z-Polym., 193, 12 (1963).

23. Heydemann, P., and Zosel, A., Acustica, 12, 360 (1962).

24. Heydemann, P., and Nagerl, H., Acustica, 14, 70 (1964).

25. Kästner, V.S., and Pohl, G., Kolloid-Z. Z-Polym., 191, 114 (1963).

26. Yee, A.F., and Takemori, M.T., ACS Polymer Preprints, 20(1), 758 (1979).

27. Yee, A.F., ACS Polymer Preprints, 21(2), 29 (1980).

28. Yee, A.F., ACS Polymer Preprints, 22(2), 285 (1981).

29. Yee, A.F., and Takemori, M.T., J. Polym. Sci. Phys. ed., 20, 205 (1982).

30. Philippoff, W., and Brodnyan, D., J. Appl Phys., 26(7), 846, (1955).

31. Koppelmann, J., Kolloid-Z, 144, 12 (1955).

32. Koppelmann, J., Rheol. Acta, 1, 20 (1958).

33. Koppelmann, J., Kolloid-Z, 164, 31 (1959).

34. Thomson, K.C., J. Appl. Polym. Sci., 10, 1133, (1966).

35. Gottenberg, W.G., and Christensen, R.M., Trans. Soc. Rheol., 7, 171 (1963).

36. Cronshaw, M.B., *Solutions of Some Relations Between Response Functions Arising in the Theory of Linear Viscoelasticity*, Master Report, California Institute of Technology, Pasadena, (1979).

37. Hopkins, I.L., and Hamming, R.W., J. Appl. Phys., 28, 906 (1957).

38. Dickie, R.A., *Mechanical Properties (Small Deformations) of Multiphase Polymer Blends*, in: D.R. Paul and S. Newman, eds., *Polymer Blends*, Academic Press, New York, 353-391 (1948).

39. Marvin, R.S., and McKinney, in: *Physical Acoustics*, W.P. Mason, ed., Vol. IIB, Academic Press, New York, (1965).

40. Marvin, R.S., Aldrich, R., and Sack, H.S., J. Appl. Phys. 25, 1213 (1954).

41. McKinney, J.E., Edelman, S., and Marvin, R.W., J. Appl. Phys., 27, 425 (1956).

42. McKinney, J. E., Belcher, H.V., and Marvin, R.S., Trans. Soc. Rheol., 4, 374 (1960).

43. McKinney, J.E., and Belcher, H.V., J. Res. Natl. Bur. Stand. Sect. A, 67A, 43 (1963).

4. Kuhn, W., Helv. Chim. Acta, 44, 927 (1961).

45. Moonan, W.K., and Tschoegl, N.W., to be submitted in Macromolecule.

46. Moonan, W.K., Ph.D. Thesis, to be submitted, California Institute of Technology, Pasadena, (1982).

47. Tschoegl, N.W., Rheol. Acta, 13, 897 (1974).

48. Kraus, G., Rollman, K.W., and Gardner, J.O., J. Polym. Sci., Polym. Phys. Ed., 10, 2061 (1972).

APPENDIX A

Analysis of the Data of Kästner and Pohl

Kästner and Pohl[25] measured the complex Young's modulus, $E^*(w)$, the complex shear modulus, $G^*(w)$, and the real part of Poisson's ratio, $\mu'(w)$ on samples of a commercial poly(methyl methacrylate) over the range of frequencies from 10^{-3} to 10^{-1} Hz and temperatures from 90°C to 115°C. The Poisson's ratio is measured in flexure utilizing the fact that the cross section of the specimen deforms in such a way that two of the sides become arcs while the other two become tilted from the undeformed plane. A mirror is attached to one of the tilting sides and the angular deflection is detected using a light beam. With this apparatus Kästner and Pohl were able to measure the real part of the Poisson's ratio, the imaginary part being below their level of detectability. The temperature variation in their measurement was ±0.2°C . The Lissajous method used does not appear to be suitable for the accurate determination of small phase angles at low frequencies.[47]

Master curves were given only for $E'(w)$, $E''(w)$, and $\mu'(w)$ but not for $G'(w)$ and $G''(w)$. No temperature shift factors were shown. We analyzed the data further to see whether $\mu'(w)$ could be calculated and whether the calculated and measured values agree reasonably. Enlargements were made on the plot of the raw data (isothermal segments). Master curves were then obtained in the usual way by superposition (see Figs. 7, 8, 9, 10, 11). The shift factors required to effect superposition are shown in Figure 12. For $\mu'(w)$, the data at 106°C were treated as if they had been taken at 105°C as for the other functions. The solid line represents the WLF equation with $c_1 = 7.14$ and $c_2 = 30.0$. Clearly shifts

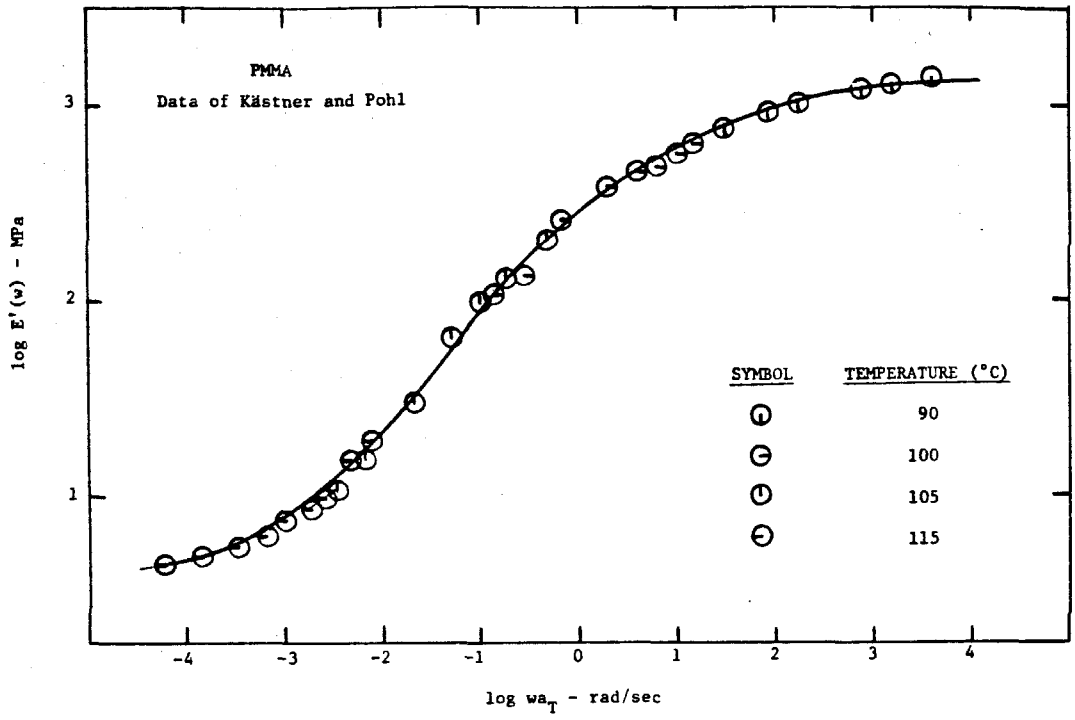

Figure 7: Master curve for real part of Young's modulus.

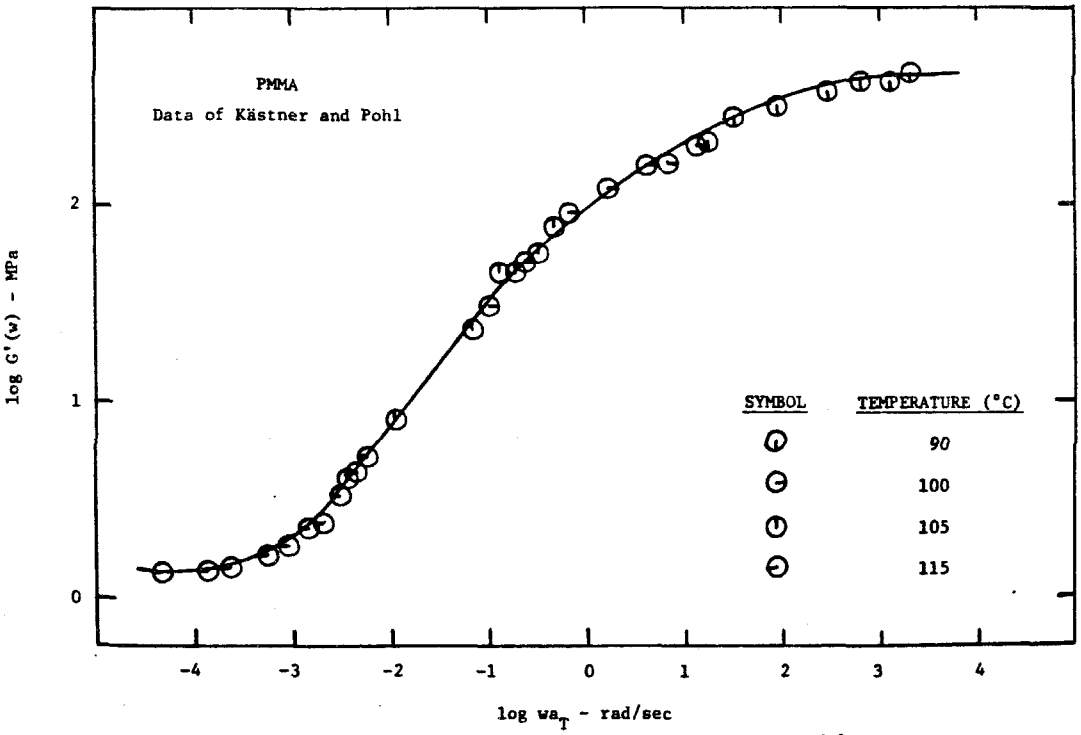

Figure 8: Master curve for real part of shear modulus.

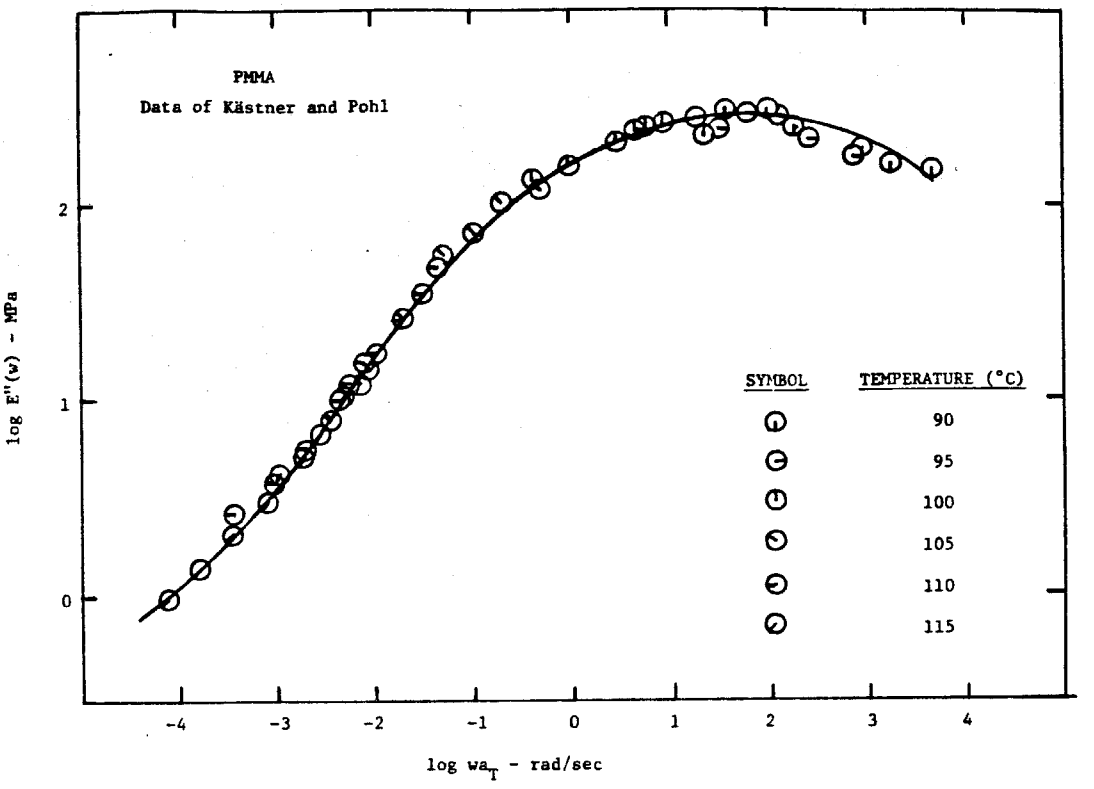

Figure 9: Master curve for imaginary part of Young's modulus.

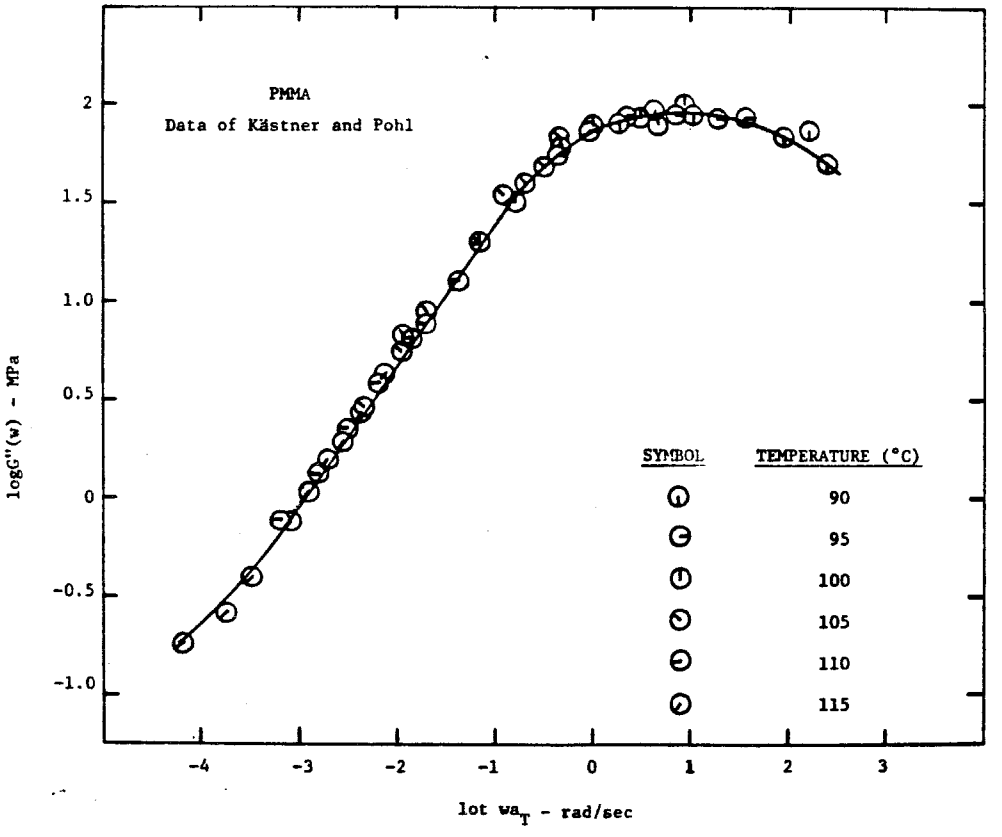

Figure 10: Master curve for imaginary part of shear modulus.

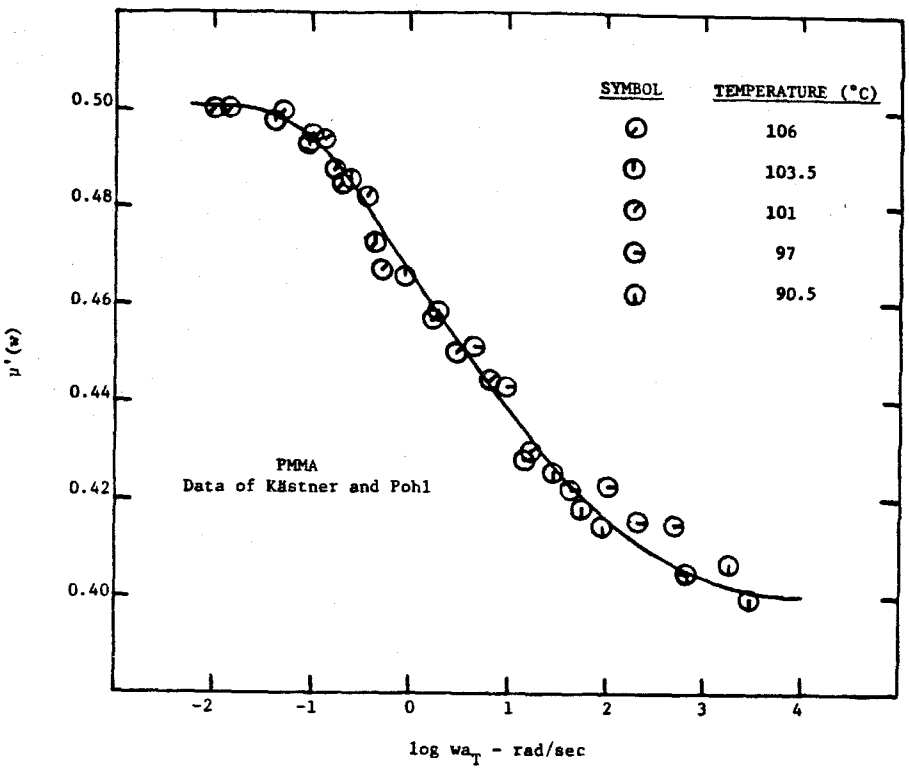

Figure 11. Master curve for real part of Poisson's ratio.

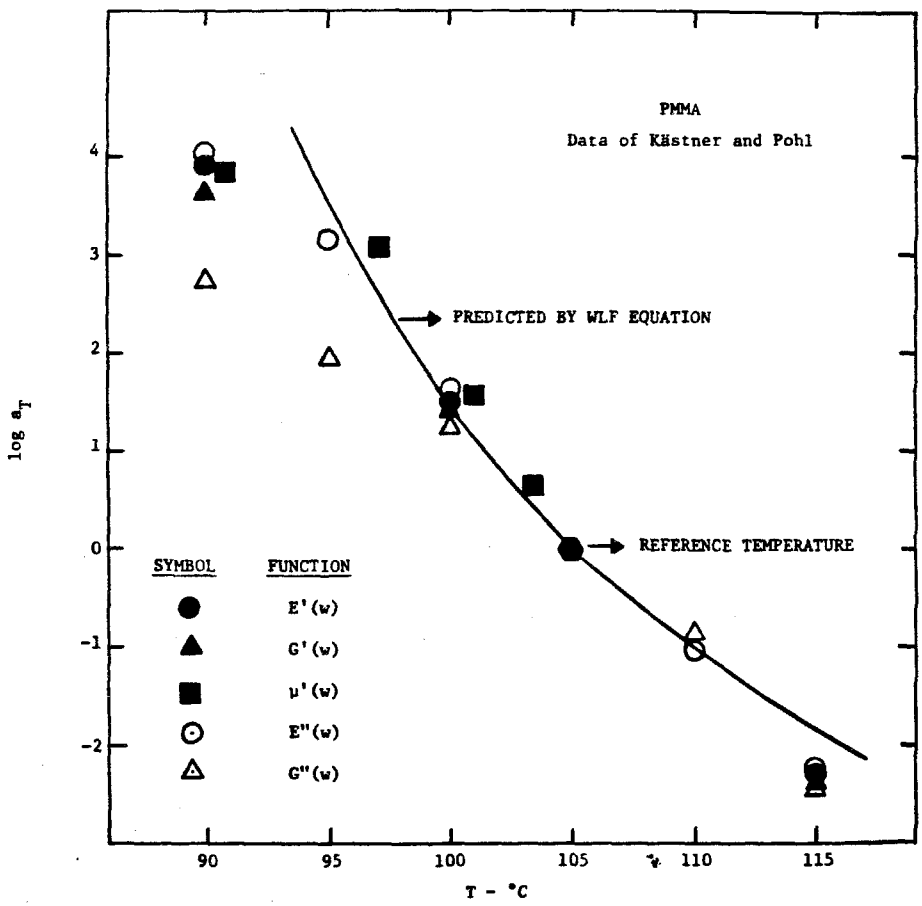

Figure 12: Shift factors as function of temperature for E'(w), E"(w), G'(w), G"(w) and μ'(w).

in the glassy regime were not consistent. This may have been caused by differences in the glasses produced through differences in the rates at which the specimens were heated or cooled.

Applying half-decade vertical shift (log 3≏0.5), E'(w) and G'(w) show reasonable agreement. The agreement is not as good when E"(w) and G"(w) are compared, particularly in the glassy region. This may be due to the difficulty of measuring small phase angles accurately, or to differences in the glasses produced. The authors inferred that the shear modulus relaxed at a higher frequency than Young's modulus but this claim does not appear to be well grounded.

Using the smoothed values of the real and imaginary components of E*(w) and G*(w), the real part of the Poisson's ratio was calculated using Eq. (5) of the Report. Figure 13 shows the calculated values of $\mu'(w)$ compared with the measured ones (smooth, solid curve). The calculated values are totally inconsistent with the measured ones. No minimum is observed in the measured values, while minima and maxima appear in the calculated values. This corroborates the finding that indirect determination of Poisson's ratio is well-nigh impossible.

Kästner and Pohl also calculated the real part of the bulk modulus, K'(w), from E*(w) and μ*(w) using the equations

$$K'(w) = \frac{1}{3} \frac{[1-2\mu'(w)]E'(w) + 2\mu''(w)E''(w)}{[1-2\mu'(w)]^2 + 4\mu''(w)^2} \qquad (1)$$

$$K''(w) = \frac{1}{3} \frac{[1-2\mu'(w)]E''(w) - 2\mu''(w)E'(w)}{[1-2\mu'(w)]^2 + 4\mu''(w)^2} \; . \qquad (2)$$

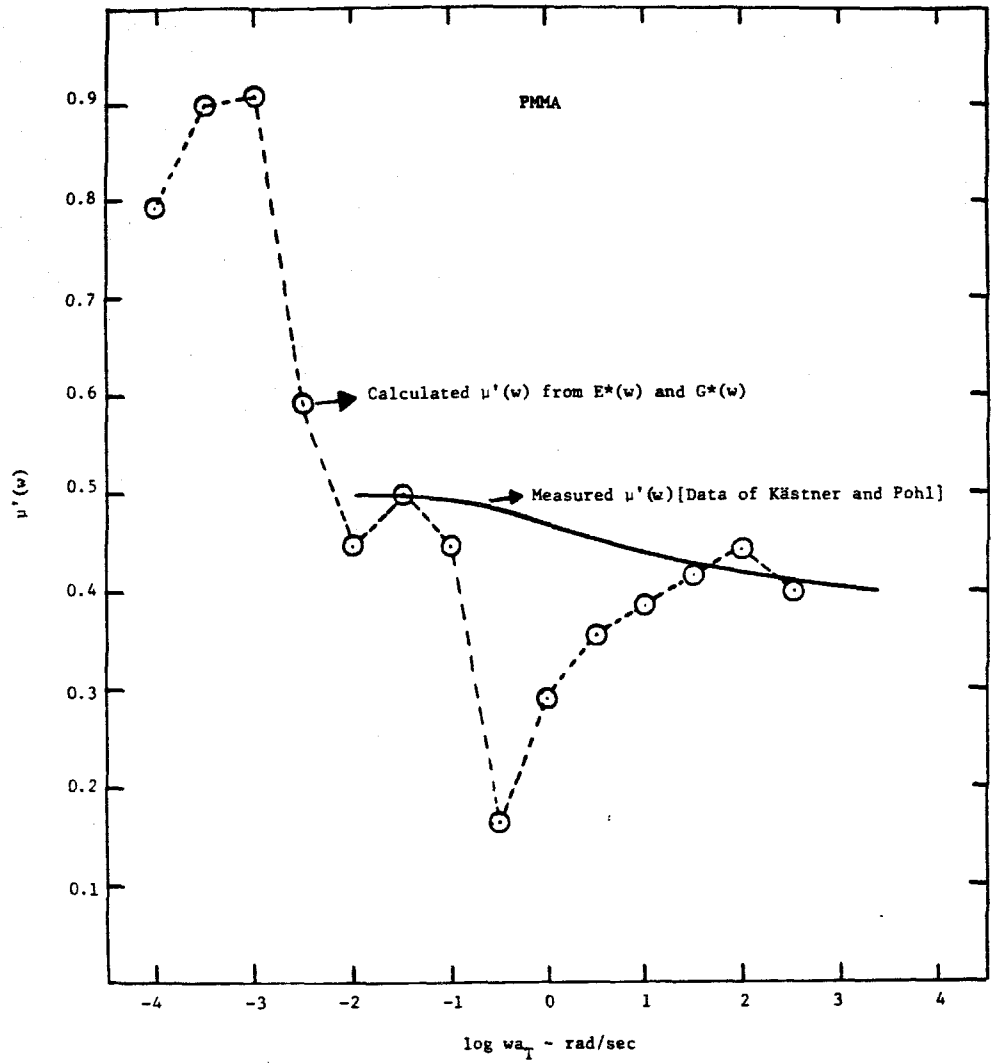

Figure 13: Comparison between calculated and measured Poisson's ratio.

Since they assume $\mu''(w) = 0$, Eqs (1) and (2) reduce to

$$K' = \frac{1}{3}\frac{E'(w)}{1-2\mu'(w)} \tag{3}$$

$$K'' = \frac{1}{3}\frac{E''(w)}{1-2\mu'(w)} \quad . \tag{4}$$

Note that Eq. (3) is essentially the equation for an elastic material (see Table 1). The authors did not calculate K"(w), nor did they calculate K'(w) and K"(w) from E*(w) and G*(w). We attempted to do so

BLANK PAGE

using the equations

$$K'(w) = \frac{[G'(w)E'(w)-G''(w)E''(w)][3G'(w)-E'(w)] + [G'(w)E''(w) + E'(w)G''(w)][3G''(w)-E''(w)]}{3\{[eG'(w)-E'(w)]^2 + [3G''(w)-E''(w)]^2\}} \quad (5)$$

$$K''(w) = \frac{[G'(w)E''(w)+E'(w)G''(w)][3G'(w)-E'(w)] - [G'(w)E'(w)-G''(w)E''(w)][3G''(w)-E''(w)]}{3\{[3G'(w)-E'(w)]^2 + [3G''(w)-E''(w)]^2\}} . \quad (6)$$

The attempt fails to produce reasonable values of K'(w) and K''(w). The calculated values of K'(w) and K''(w) oscillate from positive to negative.

This indicates that it is better to calculate K'(w) from E*(w) and μ*(w) than from E*(w) and G*(w), as already pointed out by Arridge and Crowson.[18,19] To obtain accurate values of K*(w) from E*(w) and μ*(w), one needs all four functions, E'(w), E''(w), μ'(w), and μ''(w), and these must be measured quite accurately. In the time-dependent mode only two functions, E(t) and μ(t), are needed.

APPENDIX B

The Time-Dependent Poisson's Ratio

N. W. Tschoegl

Suppose a linear viscoelastic material is subjected to a strain, ε_1, as a step function of time. The strain in the transverse direction, referred to as the *lateral contraction*, will be a function of time. Denoting this by $-\varepsilon_2(t)$, we obtain the time-dependent Poisson's ratio as

$$\mu(t) = -\varepsilon_2(t)/\varepsilon_1. \tag{1}$$

Equation (1) can be generalized to

$$-\varepsilon_2(t) = \int_0^t \mu(t-u)\,\frac{d\varepsilon_1(u)}{du}\,du. \tag{2}$$

Laplace transformation yields

$$-\bar{\varepsilon}_2(s) = s\bar{\mu}(s)\bar{\varepsilon}_1(s). \tag{3}$$

Substitution of $\bar{\varepsilon}_1(s) = \varepsilon_1/s$ and retransforming reproduces Eq. (2). Alternatively, we may write

$$-\bar{\varepsilon}_2(s) = \bar{\nu}(s)\bar{\varepsilon}_1(s) \tag{4}$$

where $\bar{\nu}(s) = s\bar{\mu}(s)$. We note that qualitatively, $\bar{\nu}(s)$ must depend on s in the same way as does the tensile retardance (the s - multiplied transform of the tensile compliance), because the lateral contraction is *delayed*

(retarded). Accordingly, we write

$$\bar{\nu}(s) = \mu_g + \Sigma_i \frac{\mu_i}{1 + \tau_i s} = \mu_e - \Sigma_i \frac{\mu_i \tau_i s}{1 + \tau_i s} \tag{5}$$

where μ_g and μ_e are the glassy and equilibrium values, and the μ_i are Poisson's ratios associated with the *delay times*, τ_i. Introducing the *Poisson* or *delay spectrum*, $m(\tau)$, we have

$$\bar{\nu}(s) = \mu_g + \int_{-\infty}^{\infty} m(\tau) \frac{1}{1 + \tau s} \, d\ln\tau \ , \tag{6}$$

where

$$\int_{-\infty}^{\infty} m(\tau) d\ln\tau = \mu_e - \mu_g \ . \tag{7}$$

We note that there is no flow term because the lateral contraction cannot proceed indefinitely even in an uncrosslinked material.

Dividing by s and retransforming we obtain

$$\mu(t) = \mu_g + \int_{-\infty}^{\infty} m(\tau)(1 - \exp -t/\tau) d\ln\tau \tag{8}$$

or

$$\mu(t) = \mu_e - \int_{-\infty}^{\infty} m(\tau) \exp -t/\tau \cdot d\ln\tau \tag{9}$$

as the time-dependent Poisson's ratio in step response.

The frequency-dependent *complex Poisson's ratio* is derived from

$$\bar{\nu}(s)\Big|_{s=j\omega} = \mu^*(\omega) = \mu'(\omega) - j\mu''(\omega) \tag{10}$$

using Eq. (6). We obtain the *storage ratio* as

$$\mu'(\omega) = \mu_g + \int_{-\infty}^{\infty} m(\tau)\, \frac{1}{1 + \omega^2\tau^2}\, d\ln\tau \tag{11}$$

and the *loss ratio* as

$$\mu''(\omega) = \int_{-\infty}^{\infty} m(\tau)\, \frac{\omega\tau}{1 + \omega^2\tau^2}\, d\ln\tau. \tag{12}$$

APPENDIX C

Calculation of the Bulk and Shear Moduli from the Tensile Modulus and Poisson's Ratio

N. W. Tschoegl

In a tensile relaxation test one measures the *stretch relaxation modulus* (or *Young's modulus*), E(t), defined by the relation

$$E(t) = \sigma_1(t)/\varepsilon_1 \tag{1}$$

where $\sigma_1(t)$ is the time dependent stress in the direction of stretch, resulting from the imposition of a step of strain, ε_1, at t = 0. The Laplace transform of Eq. (1) is

$$\bar{E}(s) = \bar{\sigma}_1(s)/\varepsilon_1. \tag{2}$$

$\bar{E}(s)$ is related to the Laplace transform of the *bulk relaxation modulus*, $\bar{K}(s)$, and the Laplace transform of the *time-dependent Poisson's ratio*, $\bar{\mu}(s)$, by

$$\bar{E}(s) = 3\bar{K}(s)[1 - 2s\bar{\mu}(s)]. \tag{3}$$

But, by definition, [cf. Eq. (1). Appen. B],

$$\bar{\mu}(s) = -\varepsilon_2(s)/\varepsilon_1 \tag{4}$$

where $-\bar{\varepsilon}_2(s)$ is the transform of the lateral contraction, i. e. the contraction in the direction transverse to the direction of stretch. Substituting Eq. (4) into (3) and using Eq. (2) gives

$$\bar{\sigma}_1(s) = 3\bar{K}(s)[\varepsilon_1 + 2s\bar{\varepsilon}_2(s)] \tag{5}$$

and retransformation yields

$$\sigma_1(t) = 3\varepsilon_1 K(t) - 6\int_0^t K(u)\,\frac{d\varepsilon_2(t-u)}{du}\,du. \tag{6}$$

Thus, if $\varepsilon_2(t)$ is determined with sufficient accuracy simultaneously with

$\sigma_1(t)$, the bulk relaxation modulus, K(t), can be recovered through numerical solution of Eq. (6).

Equation (6) expresses K(t) in terms of the experimentally observable quantities $\sigma_1(t)$ and $\varepsilon_2(t)$. Retransformation of Eq. (3)

$$E(t) = 3(1 - 2\mu_g)K(t) + 6\int_o^t K(u) \frac{d\mu\ (t-u)}{du}\, du \qquad (7)$$

where μ_g is the value of Poisson's ratio in the glassy state. Eq. (7) gives relation between the stretch and bulk relaxation moduli and the time-dependent Poisson's ratio.

Consider now the relation between the tensile relaxation modulus, the *shear relaxation modulus*, G(t), and the time-dependent Poisson's ratio. This is given in the transform plane by

$$\bar{E}(s) = 2\bar{G}(s)[1 + s\bar{\mu}(s)]. \qquad (8)$$

Using Eq. (2) and (4) this becomes

$$\bar{\sigma}_1(s) = 2\bar{G}(s)[\varepsilon_1 - s\bar{\varepsilon}_2(s)] \qquad (9)$$

which, upon retransformation, yields

$$\sigma_1(t) = 2\varepsilon_1 G(t) + 2\int_o^t G(u) \frac{d\varepsilon_2(t-u)}{du}\, du. \qquad (10)$$

Thus, the same measurements which potentially yield K(t) and $\mu(t)$ as well as E(t), should also furnish G(t). Again, the relation between E(t), G(t) and $\mu(t)$ is obtained by retransforming Eq. (8) to give

$$E(t) = 2(1 + \mu_g)G(t) - 2\int_o^t G(u) \frac{d\mu(t-u)}{du}\, du. \qquad (11)$$

Let us now consider the calculation of K(t) and G(t) from E(t) and μ(t). First, we rewrite Eq. (7) for a discrete set of n values of t and, simultaneously, subdivide the integral of integration into n subintervals. This gives

$$E(t_n) = 3(1-2\mu_g)K(t_n) + 6\sum_{i=1}^{i=n} \int_{t_{i-1}}^{t_i} K(n) \frac{d\mu(t_n-u)}{du}\, du \tag{12}$$

where $t_o = 0$. We now consider that each subinterval is small enough so that we may take out K(t) from under the integral sign with its midvalue over the subinterval. The integration can then be carried out immediately and we obtain

$$E(t_n) = 3(1-2\mu_g)K(t_n) + 3\sum_{i=1}^{i=n} [K(t_i) + K(t_{i-1})][\mu(t_n-t_i) - \mu(t_n-t_{i-1})]. \tag{13}$$

But

$$\sum_{i=1}^{i=n} K(t_{i-1})\ [\mu(t_n-t_i) - \mu(t_n-t_{i-1})] = \sum_{i=0}^{i=n-1} K(t_i)\ [\mu(t_n-t_{i+1}) - \mu(t_n-t_i)]. \tag{14}$$

Using Eq. (14) and rearranging leads to the recurrence formula

$$K(t_n) = \frac{E(t_n)/3 + K_g[\mu(t_n) - \mu(t_n-t_1)] + \sum_{i=1}^{i=n-1} K(t_i)[\mu(t_n-t_{i-1}) - \mu(t_n-t_{i+1})]}{1 - \mu_g - \mu(t_n-t_{n-1})} \tag{15}$$

with

$$K(t_1) = \frac{E(t_1)/3 + K_g[\mu(t_1) - \mu_g]}{1 - \mu_g - \mu(t_1)} \tag{16}$$

and

$$K_g = E_g/3(1-2\mu_g). \tag{17}$$

An analogous derivation proceeding from Eq. (11) leads to

$$G(t_n) = \frac{E(t_n) - G_g[\mu(t_n) - \mu(t_n-t_1)] - \sum_{i=1}^{i=n-1} G(t_i)[\mu(t_n-t_{i-1}) - \mu(t_n-t_{i+1})]}{2 + \mu_g + \mu(t_n-t_{n-1})} \tag{18}$$

with

$$G(t_1) = \frac{E(t_1) - G_g[\mu(t_1) - \mu_g]}{2 + \mu_g + \mu(t_1)} \tag{19}$$

and

$$G_g = E_g/2(1+\mu_g). \tag{20}$$

This derivation assumes that the data are equally spaced on the time scale. If, as they usually are, the data are equally spaced on the logarithmic time scale, values of $\mu(t_n-t_k)$, where $k = i-1, i, i+1, n-1$, are obtained by linear interpolation between the two closest values.

APPENDIX D

Experimental Procedure

The following is a brief rundown (checklist) of the procedure to be followed when taking measurements with stretching devices.

1. Warm up the electronic switch, the signal conditioner, the recorder, and the load cell for at least two hours to ensure the stability of the system.

2. Install the specimen in the grips. Adjust the table of the LVDT holder vertically to slightly elevate the specimen. Adjust the grips so that it is straight and the mirror should help in this adjustment.

3. Stretch the specimen once or twice with recorder on to check whether the proper output signal is detected (cf. Fig. 2). If this is not the case, check the alignment again. Do not stretch the specimen more than two percent.

4. Stretch the specimen so that the load cell output agrees with the zero elongation value for room temperature as provided from the calibration.

5. Determine the length of the specimen (gage length and bench-mark separation) using the travelling microscope. Calculate where the neutral line should fall and shift the LVDT holder horizontally so that the rod bearing the core is located on this line.

6. Remove the travelling microscope to prevent damages of the lenses at very high and low temperatures.

7. Set the thermotrol to the desired temperature. Close the tank and the environmental chamber, and start the temperature servo. Monitor the air and bath temperature using thermocouples. Wait until the desired bath temperature has become stable.

8. Set the gain on the electronic switch as required for the measurements at the test temperature. In the rubbery and glassy regions set the gain to 50 or above. Lower the gain progressively as the transition region is approached.

9. Set the recorder to the appropriate scale. For the load cell output set 2 mV full scale in the rubbery region and increase it to 5 mV full scale through the transition region to the glassy region. For the LVDT output set the recorder gain to 1 volt full scale.

10. Short-circuit the input to the electronic switch, with short length of cables. Push the "SAMPLE" button on the panel and connect the output to the recorder. Locate the recorder pens at (1/10)th of full scale. This is the base line for the electronic switch. Every other voltage measurement must be referred to this line.

11. Now disconnect the shorting cables and reconnect the load cell and the LVDT output back to electronic switch.

12. Note the bath temperature.

13. Adjust the LVDT output using zero adjust on the CAS to slightly larger than zero as seen on the digital display of the electronic switch. Push the "SAMPLE" button, note the gain, the digital display, the recorder speed, and the full scale reading for both the LVDT and the load cell.

14. Run the recorder and stretch the specimen. Note the digital display after stretching. If the gain is set too high, the pen will go out of scale. Then push the "SAMPLE" button and re-record the digital displays.

15. Wait until the signal outputs have become steady (relaxation is effectively over). Now push the "SAMPLE" button again and note the digital displays. These numbers will be used only to double-check the change in output of the LVDT and the load cell.

16. Open the environmental chamber, reinstall the travelling microscrope and measure the final length of the specimen (both gage length and bench mark separation).

17. Return the specimen to its original elongation, allow it to relax and then repeat the same procedure for the next measurement.

APPENDIX E

Circuit and Wiring Diagrams of the Electronic Switch

MODIFICATION TO MINARIK SLF63 MOTOR CONTROLLER:

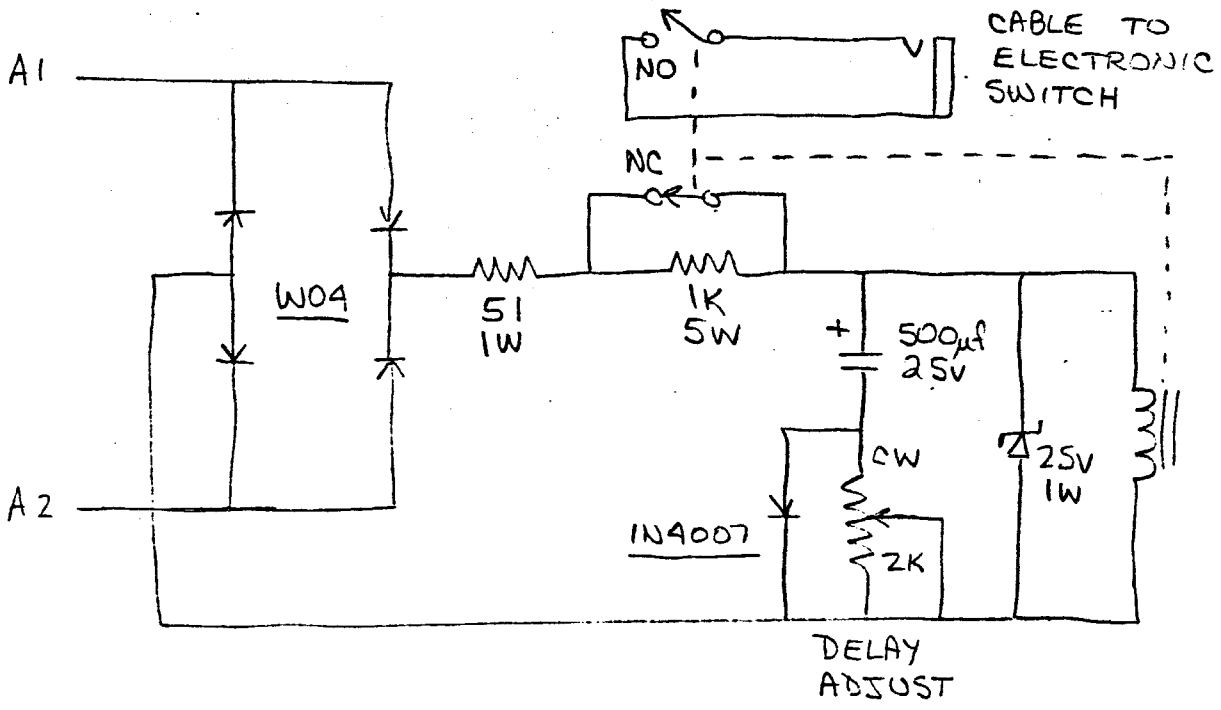

RELAY: DELTROL
24 VDC
DPDT

A1, A2: TERMINALS ON STRIP INSIDE BOX.

POWER SUPPLY CONNECTION BOX FOR LOAD CELL.

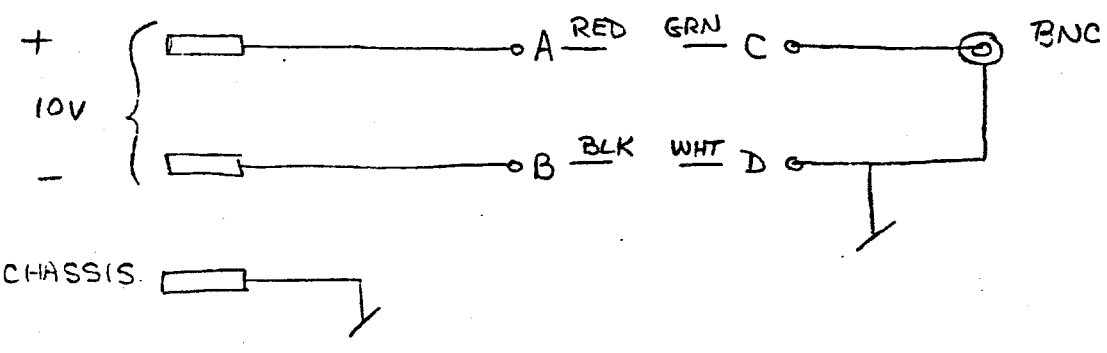

ELECTRONIC SWITCH

10/29/81

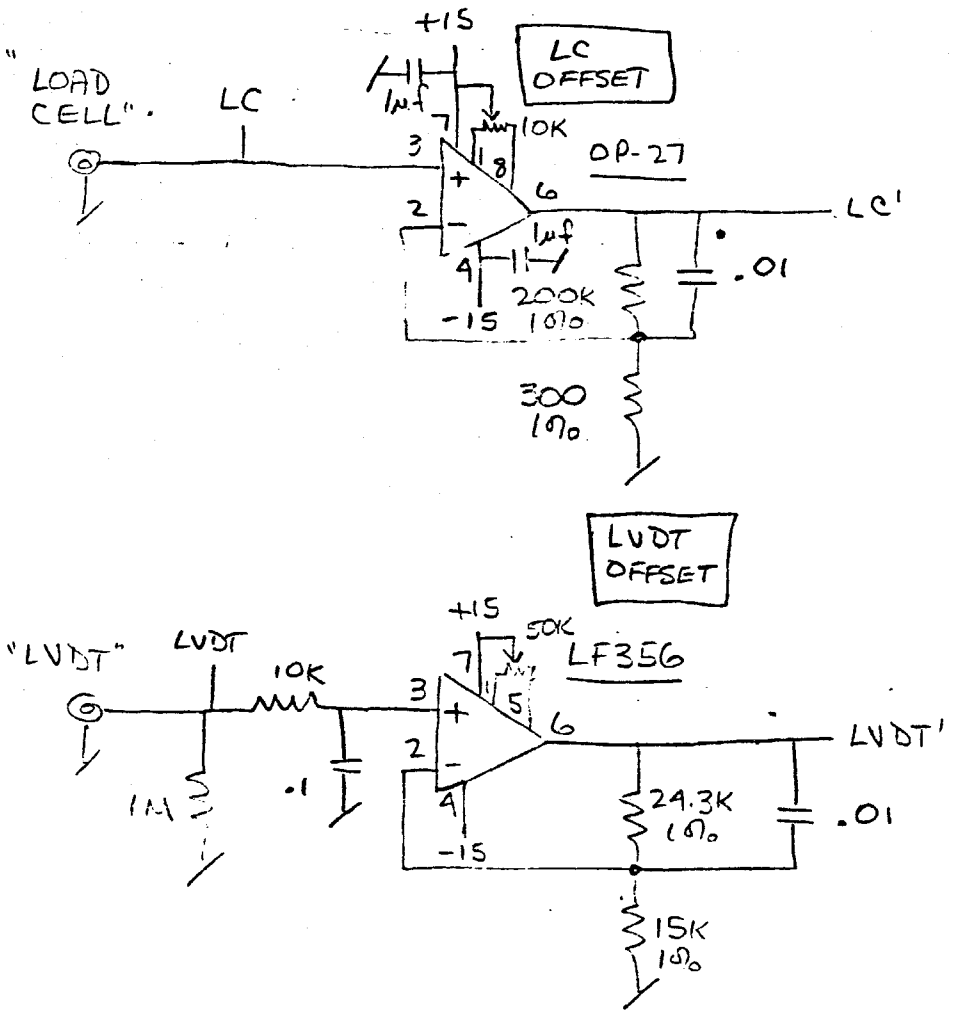

	ELECTRONIC SWITCH	ADC	11/13/81

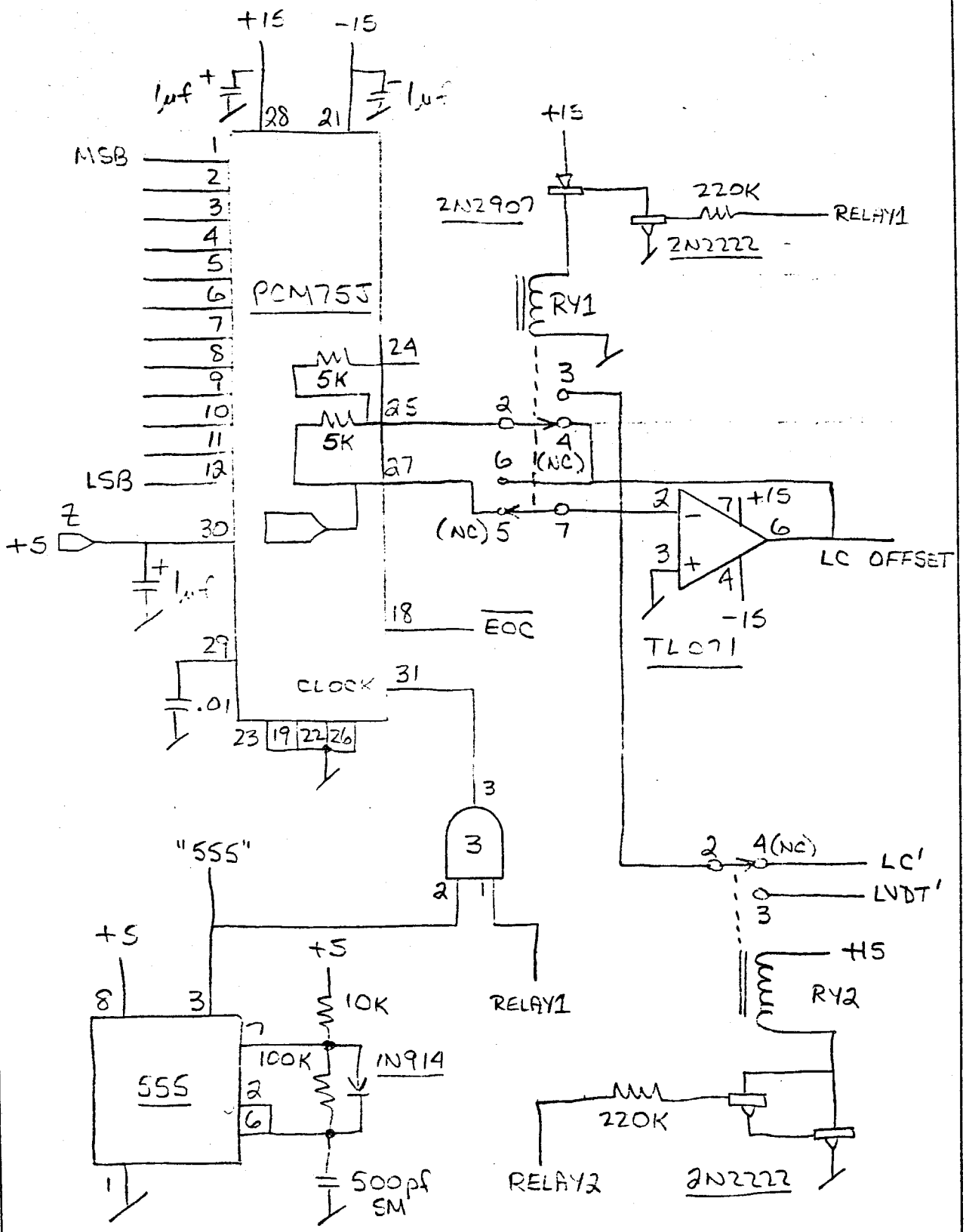

ELECTRONIC SWITCH

10/29/81

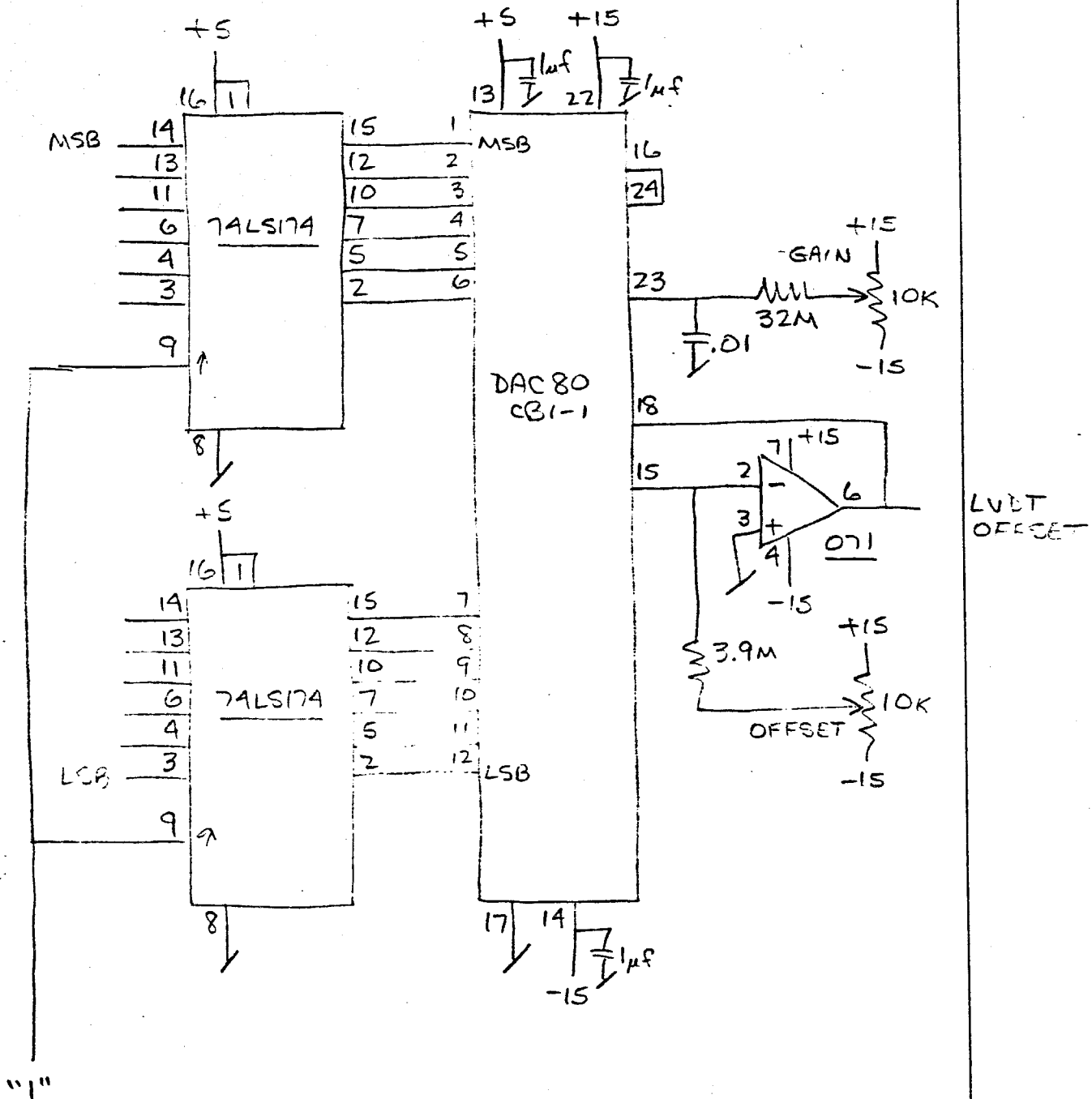

ELECTRONIC SWITCH

11/30/81

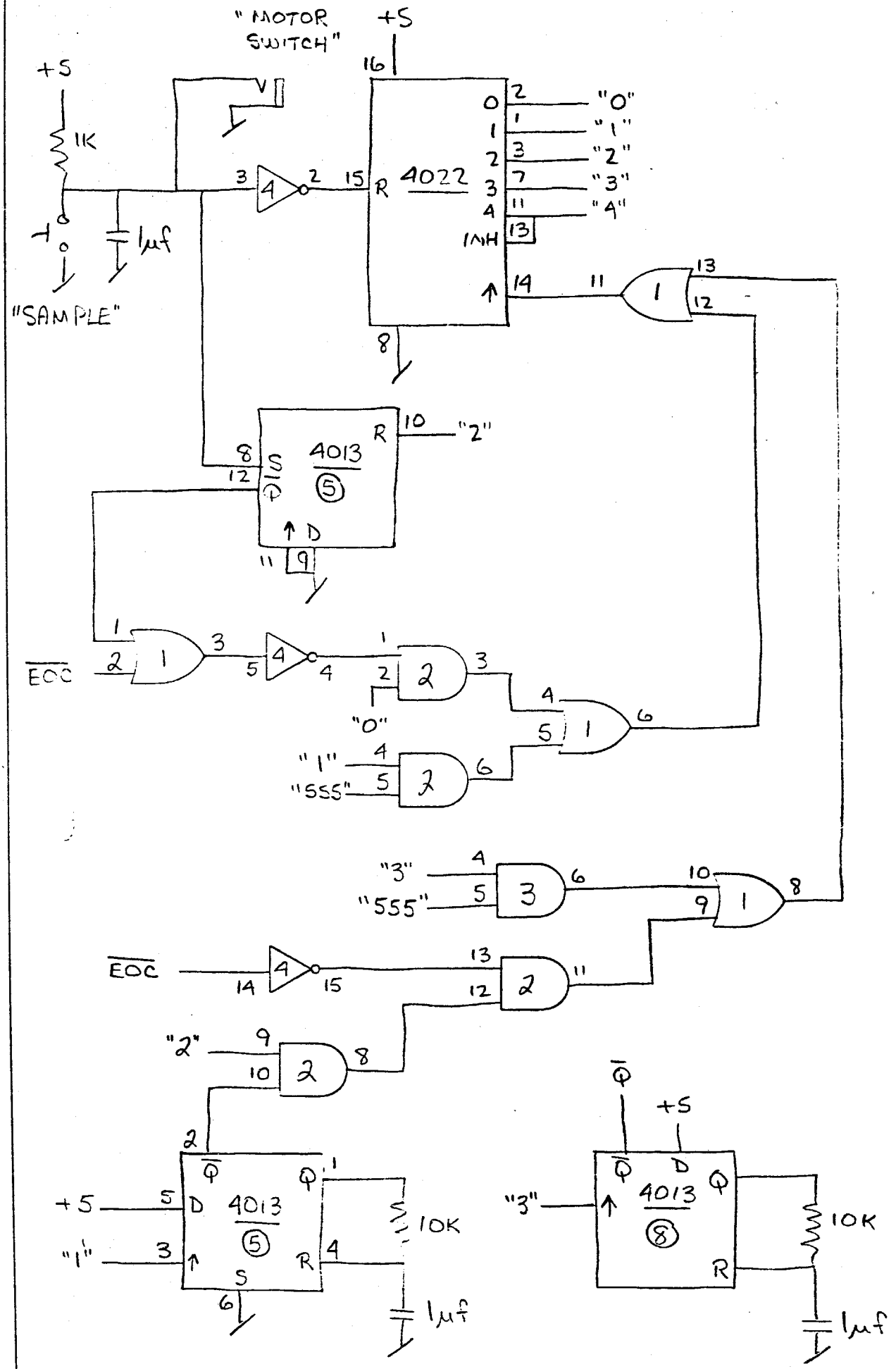

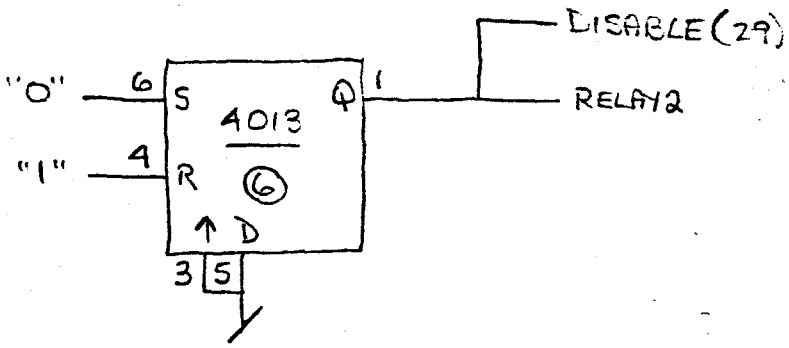
DISABLE (29)
"0"
6
S
4013
Q
1
RELAY2
"1"
4
R
⑥
↑ D
3
5

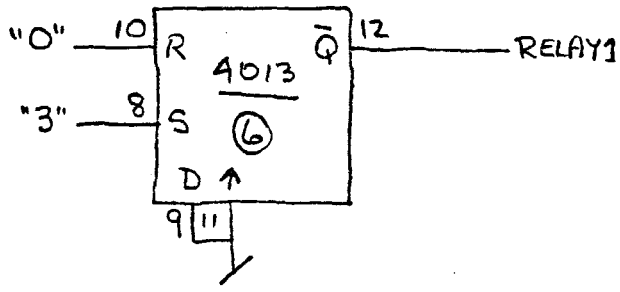
"0"
10
R
4013
Q̄
12
RELAY1
"3"
8
S
⑥
D ↑
9
11

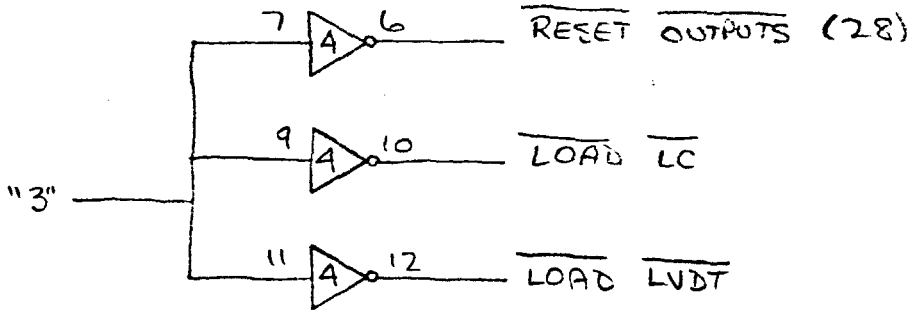
7
4
6
RESET OUTPUTS (28)
9
4
10
LOAD LC
"3"
11
4
12
LOAD LVDT

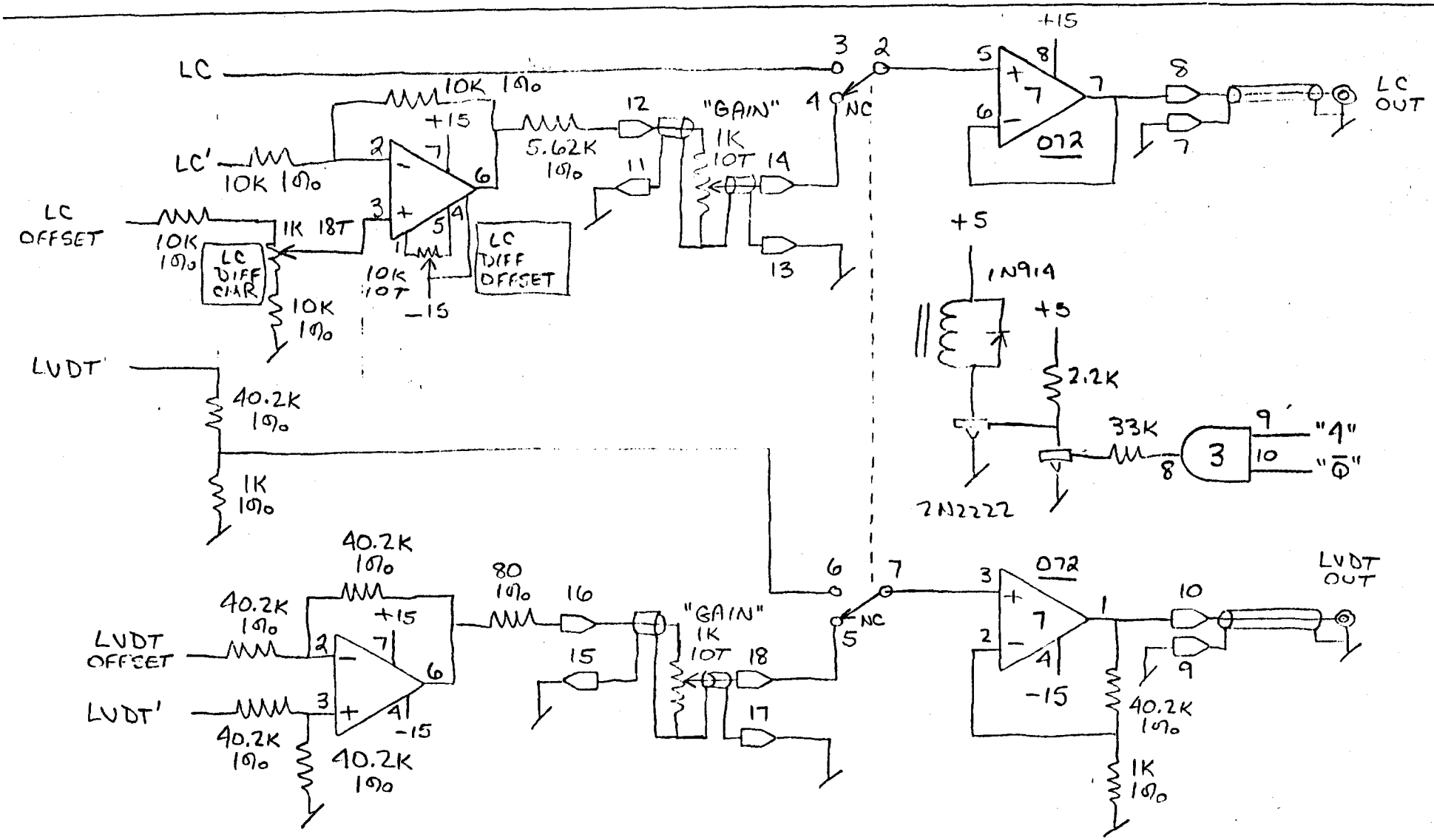
LC
10K 1%
+15
LC'
10K 1%
2
7
6
3
4
5
1
10K 10T
-15
LC DIFF CHAR
LC DIFF OFFSET
LC OFFSET
10K 1%
1K 18T
10K 1%
5.62K 1%
12
11
"GAIN"
1K 10T
14
13
3
2
4
NC
+15
5
8
7
6
072
7
8
LC OUT
+5
1N914
2.2K
33K
9
"1"
10
"0"
8
3
2N2222
LVDT
40.2K 1%
1K 1%
40.2K 1%
80 1%
16
15
"GAIN"
1K 10T
18
17
6
5
NC
7
LVDT OFFSET
LVDT'
40.2K 1%
40.2K 1%
-15
072
3
2
7
1
4
10
9
-15
40.2K 1%
1K 1%
LVDT OUT

AMSLEY CONNECTOR

1	GND		
2	ADC - LSB	LOAD CELL	
3	" 1		
4	" 2		
5	" 3		
6	" 4		
7	" 5		
8	" 6		
9	" 7		
10	" 8		
11	" 9		
12	" 10		
13	" MSB		
14	GND		
15	DAC - LSB	LVDT	
16	" 1		
17	" 2		
18	" 3		
19	" 4		
20	" 5		
21	DAC - 6	LVDT	
22	" 7		
23	" 8		
24	" 9		
25	" 10		
26	" MSB		
27	GND		
28	$\overline{\text{RESET}}$ DISPLAYS		
29	DISABLE DISPLAYS		
30	$\overline{\text{STORE}}$ OUTPUT		
31	CLOCK		
32			
33			
34			
35			
36			
37			
38			
39			
40	GND		

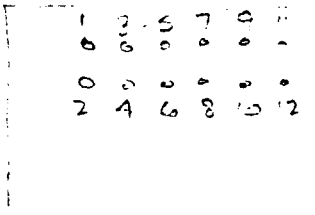

BOTTOM VIEW

EDGE CONNECTOR

1	GND	17	GND
2	LOAD CELL	18	LVDT GAIN OUT
3	GND		
4	LVDT	A	GND
5	GND	K	+15
6	SWITCH	L	GND
7	GND	M	-15
8	LC OUT	7	+5
9	GND		
10	LVDT OUT		
11	GND		
12	LC GAIN IN		
13	GND		
14	LC GAIN OUT		
15	GND		
16	LVDT GAIN IN		

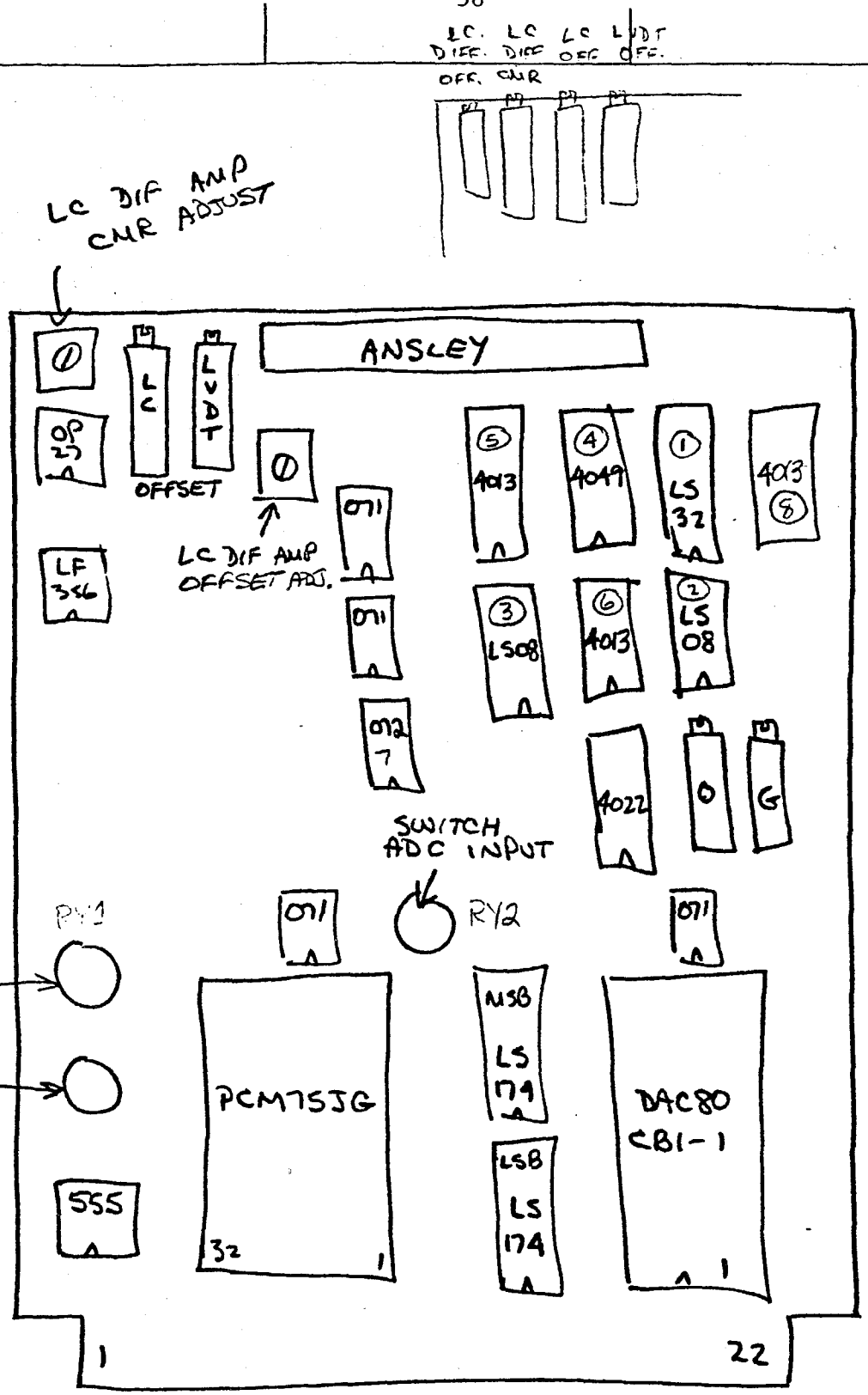
LC. LC LC LVDT
DIFF. DIFF OFF OFF.
OFF. CMR
LC DIF AMP
CMR ADJUST
ANSLEY
OP 27
LC
LVDT
OFFSET
LC DIF AMP
OFFSET ADJ.
LF 356
071
071
072
7
4013
4049
LS 32
4013
LS08
4013
LS 08
4022
SWITCH
ADC INPUT
RY1
RY2
071
071
PCM75JG
32
1
MSB
LS 174
LSB
LS 174
DAC80
CBI-1
1
555
1
22

TOP VIEW

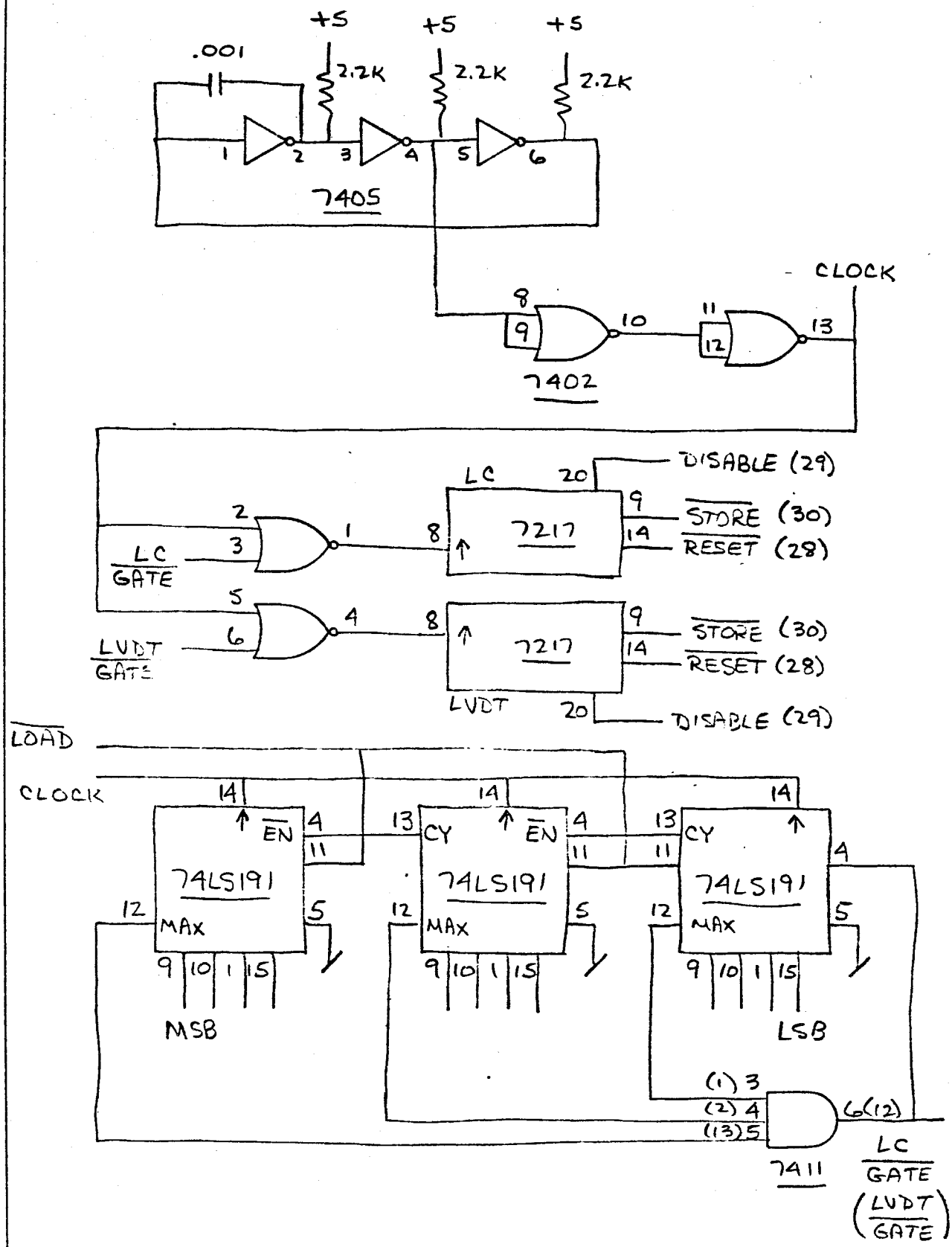
+5
+5
+5
.001
2.2K
2.2K
2.2K
1
2
3
4
5
6
7405
CLOCK
8
9
10
11
12
13
7402
LC
20
DISABLE (29)
2
3
1
8
7217
9
14
STORE (30)
RESET (28)
LC GATE
5
6
4
8
7217
LVDT
20
DISABLE (29)
LVDT GATE
LOAD
CLOCK
14
EN
4
11
13
CY
74LS191
12
MAX
5
9
10
1
15
MSB
LSB
(1) 3
(2) 4
(13) 5
6(12)
7411
LC GATE
(LVDT GATE)

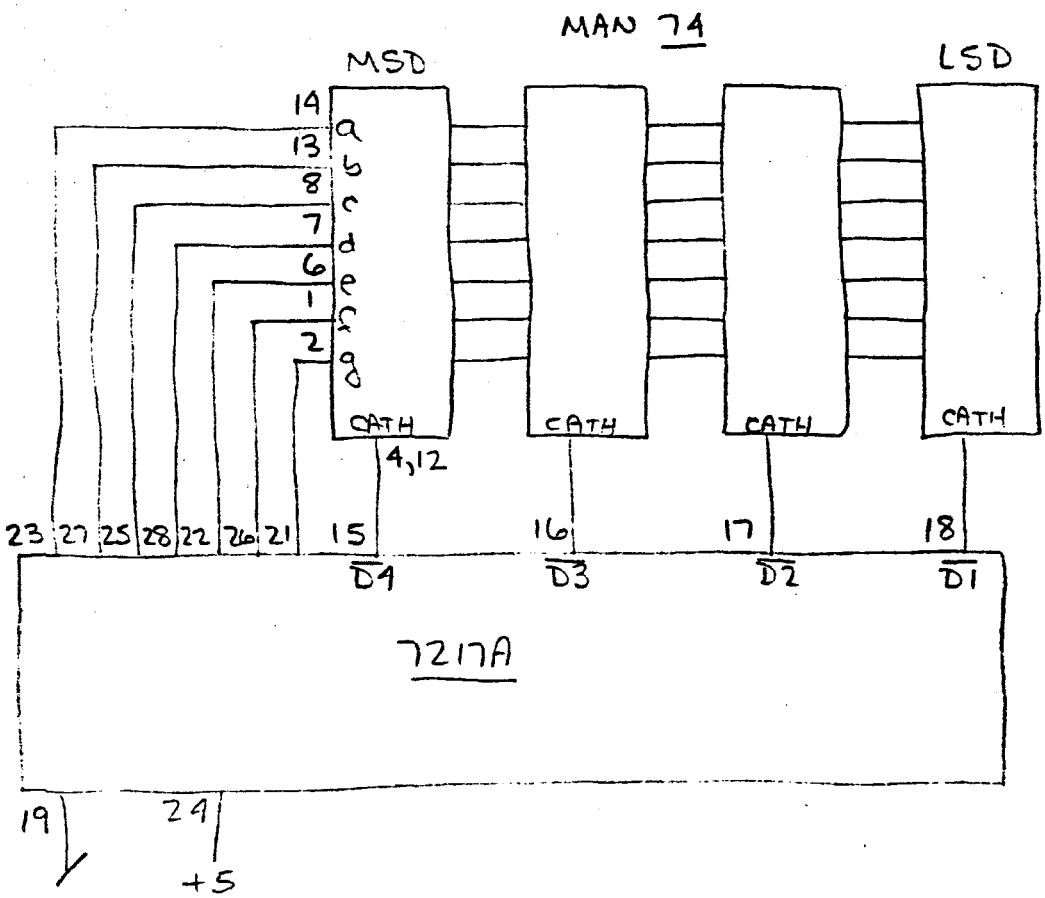
MAN 74
MSD
LSD
14
13
8
7
6
1
2
a
b
c
d
e
f
g
CATH
CATH
CATH
CATH
4,12
23
27
25
28
22
26
21
15
16
17
18
D4
D3
D2
D1
7217A
19
24
+5

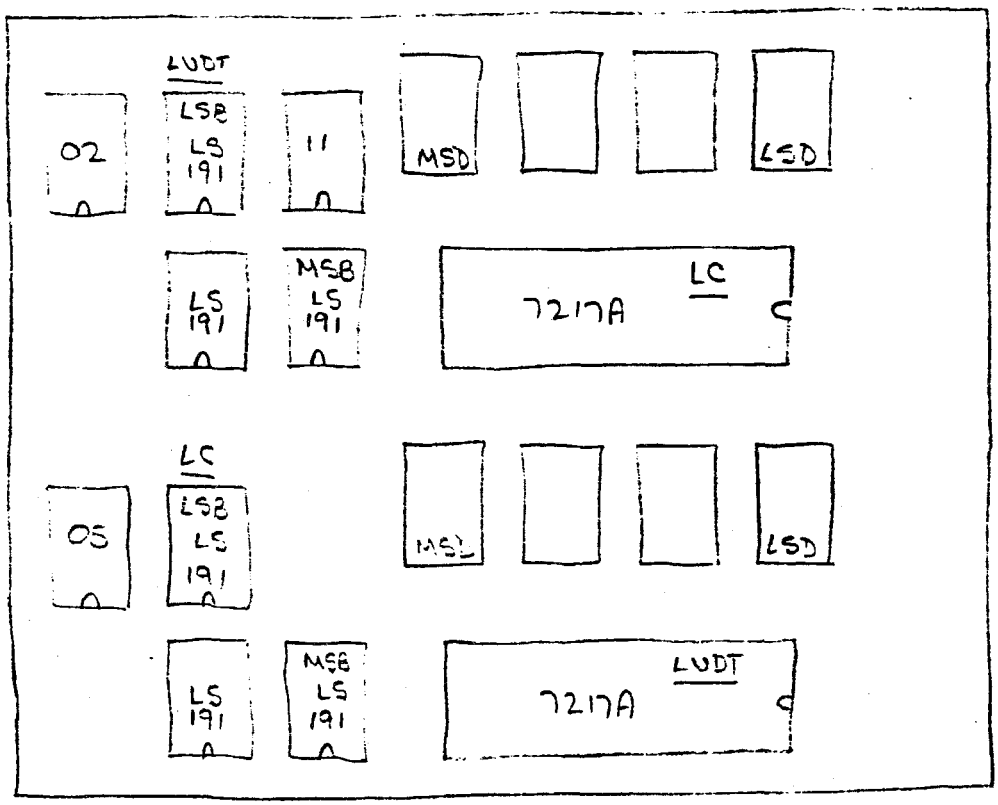
LUDT
LSB
LS 191
02
11
MSD
LSD
LS 191
MSB
LS 191
7217A
LC
LC
LSB
LS 191
05
MSD
LSD
LS 191
MSB
LS 191
7217A
LUDT

11/12/

LOAD CELL (GAIN = 5)

IN	OFFSET	OUTPUT (DN)	OUTPUT (UP)
0	5	+2.13mV	+2.16mV
1 mV	274	+3.13	+2.15 mV
2	546	+4.14	+2.15
3	819	+5.13	+2.15
4	1090	+6.14	+2.15
5	1364	+7.27	+2.19
6	1636	+8.32	+2.24
7	1907	+9.57	+2.26
8	2180	+10.63	+2.24
9	2451	+11.73	+2.25
10	2720	+12.79	+2.25
11	2994	+13.81	+2.26
12	3267	+14.71	+2.25
13	3541	+15.70	+2.24
14	3813	+16.85	+2.23
15	4085	+17.92	+2.15

3.67×10^{-6} VOLT/COUNT

INPUT: 3mV +2.06 mV
GAIN: 20 (51)
ΔV = 1mV −48.92
+2.17

IN	OFFSET	OUTPUT (DN)	OUTPUT (UP)
0	0	+.050	+.115
+.5	538	+.550	+.105
+1	1074	+1.050	+.112
+1.5	1611	+1.551	+.110
+2	2148	+2.141	+.112
+2.5	2685	+2.552	+.101
+3	3222	+3.181	+.119
+3.5	3758	+3.703	+.161

9.31×10^{-4} VOLT/COUNT

5.255 ⇒ ~~52.55 @ 50~~
70.27 @ 70
10.02 @ 10
40.24 @ 40
50.21 @ 50
90.35 @ 90